A general theoretical scheme for shape-programming of incompressible hyperelastic shells through differential growth

Zhanfeng Li[a], Jiong Wang[a,b,*], Mokarram Hossain[c], Chennakesava Kadapa[d]

[a]*School of Civil Engineering and Transportation, South China University of Technology, 510640 Guangzhou, China*
[b]*State Key Laboratory of Subtropical Building Science, South China University of Technology, 510640 Guangzhou, China*
[c]*Zienkiewicz Centre for Computational Engineering (ZCCE), Swansea University, Swansea SA1 8EN, United Kingdom*
[d]*School of Engineering and the Built Environment, Edinburgh Napier University, Edinburgh EH10 5DT, United Kingdom*

Abstract

In this paper, we study the problem of shape-programming of incompressible hyperelastic shells through differential growth. The aim of the current work is to determine one of the possible growth tensors (or growth functions) that can produce the deformation of a shell to the desired shape. First, a consistent finite-strain shell theory is introduced. The shell equation system is established from the 3D governing system through a series expansion and truncation approach. Based on the shell theory, the problem of shape-programming is studied under the stress-free assumption. For a special case in which the parametric coordinate curves generate a net of curvature lines on the target surface, the sufficient condition to ensure the vanishing of the stress

*Corresponding author. Tel.: +86 13926459861, Fax: +86 21-87114460.
Email addresses: `ctzf.li@mail.scut.edu.cn` (Zhanfeng Li), `ctjwang@scut.edu.cn` (Jiong Wang), `mokarram.hossain@swansea.ac.uk` (Mokarram Hossain), `c.kadapa@napier.ac.uk` (Chennakesava Kadapa)

components is analyzed, from which the explicit expression of the growth tensor can be derived. In the general case, we conduct the variable changes and derive the total growth tensor by considering a two-step deformation of the shell. With these obtained results, a general theoretical scheme for shape-programming of thin hyperelastic shells through differential growth is proposed. To demonstrate the feasibility and efficiency of the proposed scheme, several typical examples are studied. The derived growth tensors in these examples have also been implemented in the numerical simulations to verify their correctness and accuracy. The simulation results show that the target shapes of the shell samples can be recovered completely. The scheme for shape-programming proposed in the current work is helpful in designing and manufacturing intelligent soft devices.

1. Introduction

Growth of soft biological tissues and swelling (or expansion) of soft polymeric gels are commonly observed in nature (Ambrosi et al., 2011; Liu et al., 2015). Due to the inhomogeneity or incompatibility of the growth fields, soft material samples usually exhibit diverse morphological changes and surface pattern evolutions during the growing processes, which is referred to as the 'differential growth' and has attracted extensive research interest in recent years (Goriely and Ben Amar, 2005; Li et al., 2012; Kempaiah and Nie, 2014; Huang et al., 2018). To fulfill the requirements of engineering applications, it is usually desired that the configurations of soft material samples are con-

trollable during the growing processes, such that certain kinds of functions are realized. This goal can be achieved through sophisticated composition or architectural design in the soft material samples. The technique is known as 'shape-programming' (Liu et al., 2016; van Manen et al., 2018), which has been utilized for manufacturing a variety of intelligent soft devices, e.g., biomimetic 4D printing of flowers (Gladman et al., 2016), pressure-actuated deforming plate (Siéfert et al., 2019), pasta with transient morphing effect (Tao et al., 2021), and polymorphic metal-elastomer composite (Hwang et al., 2022).

From the viewpoint of solid mechanics, soft materials can be treated as certain kinds of hyperelastic materials. The growth field in a soft material sample is usually modeled by incorporating a growth tensor. Due to the residual stresses triggered by the incompatibility of the growth field, as well as the external loads and boundary restrictions, the sample also undergoes elastic deformations. Thus, the total deformation gradient tensor should be decomposed into an elastic strain tensor and a growth tensor (Kondaurov and Nikitin, 1987; Rodriguez et al., 1994; Ben Amar and Goriely, 2005). The elastic incompressible constraint should also be adopted since the elastic deformations of soft materials are typically isochoric (Wex et al., 2015; Kadapa et al., 2021). Based on these constitutive and kinematic assumptions, the growth behaviors of soft material samples can be studied by solving the system of mechanical field equations. Because of the inherent nonlinearities in the large growth-induced deformations, mechanical instabilities can also be triggered in the soft material samples (Ben Amar and Goriely, 2005; Li et al., 2011; Goriely, 2017; Pezzulla et al., 2018; Xu et al., 2020).

Despite the numerous studies on the growth behaviors of soft material samples, the majority of the modeling works pay attention to the direct problem, i.e., determining the deformations of soft material samples when the growth fields are specified. However, in order to utilize the shape-programming technique for engineering applications, one also needs to study the inverse problem. That is, how to determine the growth fields in the samples such that the current configurations induced by differential growth can achieve certain target shapes? This inverse problem has also been studied in some previous works (cf. Dias et al., 2011; Jones and Mahadevan, 2015; van Rees et al., 2017; Acharya, 2019; Wang et al., 2019a; Nojoomi et al., 2021; Li et al., 2022; Wang et al., 2022). In these works, the initial configurations of soft material samples usually have the thin plate form. Although the shell form is more common in nature and engineering fields, it is seldom chosen as the initial configuration of the soft material samples due to the difficulties associated with modelling shell structures. Besides that, the growth fields (or growth functions) in the samples are usually determined through the numerical and optimization approach. From the obtained numerical results, it is not convenient to find out the relations between the growth functions and the target geometrical shapes of the samples. To our knowledge, the explicit analytical results for shape-programming of soft material samples are still rare in the literature. Furthermore, the growth fields obtained in some works are represented by the tensors with general/complicated forms, which are difficult to be realized in practical conditions.

To achieve the goal of shape-programming, a prerequisite is to predict the relations between the growth fields and the morphologies of soft mate-

4

rial samples. It is thus of significance to establish an efficient and accurate mathematical model by taking configurations of samples, material properties, boundary conditions and other factors into account. In terms of shell theories for growth deformations, the Kirchhoff shell theory has been adopted to describe mechanical behavior in growing soft membranes (Vetter et al., 2013; Rausch and Kuhl, 2014), which relies on *ad hoc* assumptions of the stress components and deformation gradient. Another shell theory is proposed based on the non-Euclidean geometry, where the deformation of samples is determined by the intrinsic geometric properties attached to surfaces, such as the first and second fundamental forms, and the applied growth fields (Souhayl Sadik et al., 2016; Pezzulla et al., 2018). In Song and Dai (2016), a consistent finite-strain shell theory has been proposed within the framework of nonlinear elasticity, where the shell equation is derived from the 3D formulation through a series-expansion and truncation approach. This approach has been extended in Li et al. (2019) to derive a finite-strain shell theory for incompressible hyperelastic materials and in Yu et al. (2020) to establish a consistent dynamic finite-strain shell theory. To apply this theory for growth-induced deformations, Yu et al. (2022) incorporated the growth effect through the decomposition of the deformation gradient and derived the shell equation system for soft shell samples.

In this paper, we aim to propose a general theoretical scheme for shape-programming of incompressible hyperelastic shells through differential growth. Following the shell theory proposed in Yu et al. (2022), the shell equation system is established from the 3D governing system, where a series expansion and truncation approach is adopted. To fulfill the purpose of shape-

programming, the shell equation system is tackled by assuming that all the stress components vanish. Under this stress-free assumption, we first consider a special case in which the parametric coordinate curves generate a net of curvature lines on the target surface. By analyzing the sufficient condition to ensure the vanishing of the stress components, the explicit expression of the growth tensor is derived (i.e., the inverse problem is solved), which depends on the intrinsic geometric properties of the target surface. In the general case that the parametric coordinate curves cannot generate a net of curvature lines on the target surface, we conduct the variable changes and derive the total growth tensor by considering a two-step deformation of the shell sample. Based on these results, a theoretical scheme for shape-programming of hyperelastic shells is formulated. The feasibility and efficiency of this scheme are demonstrated by studying several typical examples.

Compared with the previous works on shape-programming of soft material samples, our current work has the following advantages:

- We solve the problem of shape-programming for thin hyperelastic shells, i.e., the initial configurations of the samples have general 3D shell forms and they can change to another 3D shell forms through differential growth.

- We derive the explicit analytical formulas for shape-programming of thin hyperelastic shells, from which the relations between the growth functions and the geometrical properties of the target configurations of the samples can be seen clearly. Besides that, it can be proved that these formulas are satisfied for the shells made of different kinds of hyperelastic materials.

- The obtained growth tensors have simple forms (cf. the diagonal forms of $\mathbb{G}$ in Eq. (45) and $\mathbb{G}_1$ in Eq. (57)), which are easier to be realized in practical conditions.

This paper is organized as follows. In section 2, the finite-strain shell theory for modeling the growth behaviors of thin hyperelastic shells is introduced. In section 3, the problem of shape programming is solved and the theoretical scheme is proposed. In section 4, some typical examples are studied to show the efficiency of the theoretical scheme. Finally, some conclusions are drawn. In the following notations, the Greek letters $(\alpha, \beta, \gamma ...)$ run from 1 to 2, and the Latin letters $(i, j, k...)$ run from 1 to 3. The repeated summation convention is employed and a comma preceding indices $(\cdot)_,$ represents the differentiation.

2. The finite-strain shell theory

In this section, we first formulate the 3D governing system for modeling the growth behavior of a thin hyperelastic shell. Then, through a series-expansion and truncation approach, the finite-strain shell equation system of growth will be established.

2.1. Kinematics and the 3D governing system

We consider a thin homogeneous hyperelastic shell locating in the three-dimensional (3D) Euclidean space R^3. Within an orthonormal frame $\{O; \mathbf{e}_1, \mathbf{e}_2, \mathbf{e}_3\}$, the reference configuration of the shell occupies the region $\mathcal{K}_r = \mathcal{S}_r \times [0, 2h]$, where the thickness parameter h is much smaller than the dimensions of

7

the base (bottom) surface $\mathcal{S}_r$ and its local radius of curvature. The position vector of a material point in the reference configuration $\mathcal{K}_r$ is denoted by $\mathbf{X} = X^i \mathbf{e}_i$ (cf. Fig. 1a). The geometric description of a shell has been systematically reported in the literature (cf. Ciarlet, 2005; Steigmann, 2012; Song and Dai, 2016), which is simply introduced below.

First, a curvilinear coordinate system $\{\theta^\alpha\}_{\alpha=1,2}$ is utilized to parametrize the base surface $\mathcal{S}_r$ of the shell in the reference configuration, which yields the parametric equation as

$$\mathbf{s}(\theta^\alpha) = \left\{ X^1(\theta^\alpha), X^2(\theta^\alpha), X^3(\theta^\alpha) \right\}, \quad (\theta^\alpha)_{\alpha=1,2} \in \Omega_r. \tag{1}$$

This parametric equation represents a continuous map from the region $\Omega_r \subset R^2$ to the surface $\mathcal{S}_r \subset R^3$. At a generic point on $\mathcal{S}_r$, the tangent vectors along the coordinate curves are given by $\mathbf{g}_\alpha = \mathbf{s}_{,\alpha} = \partial \mathbf{s}/\partial \theta^\alpha$, which span the tangent plane to the surface $\mathcal{S}_r$ at that point. The two vectors $\{\mathbf{g}_\alpha\}_{\alpha=1,2}$ are also referred to as the covariant basis of the tangent plane. Another two vectors $\{\mathbf{g}^\alpha\}_{\alpha=1,2}$ on the tangent plane can be determined unambiguously through the relations $\mathbf{g}_\alpha \cdot \mathbf{g}^\beta = \delta_\alpha^\beta$, which form the contravariant basis of the tangent plane. Then, the unit normal vector of the surface $\mathcal{S}_r$ should be defined by $\mathbf{n} = (\mathbf{g}_1 \wedge \mathbf{g}_2)/|\mathbf{g}_1 \wedge \mathbf{g}_2|$ (cf. Fig. 1b). By denoting $\mathbf{g}_3 = \mathbf{g}^3 = \mathbf{n}$, $\{\mathbf{g}_i\}_{i=1,2,3}$ and $\{\mathbf{g}^i\}_{i=1,2,3}$ constitute two sets of right-handed orthogonal bases on the base surface $\mathcal{S}_r$. The first and second fundamental forms of the surface $\mathcal{S}_r$ can be written into

$$\mathrm{I}_r = g_{\alpha\beta} d\theta^\alpha d\theta^\beta, \quad \mathrm{II}_r = b_{\alpha\beta} d\theta^\alpha d\theta^\beta, \tag{2}$$

where $g_{\alpha\beta} = \mathbf{g}_\alpha \cdot \mathbf{g}_\beta$ and $b_{\alpha\beta} = \mathbf{s}_{,\alpha\beta} \cdot \mathbf{n}$ are the fundamental quantities.

Conventionally, the fundamental quantities are also denoted by

$$E_r = g_{11}, \quad F_r = g_{12} = g_{21}, \quad G_r = g_{22},$$

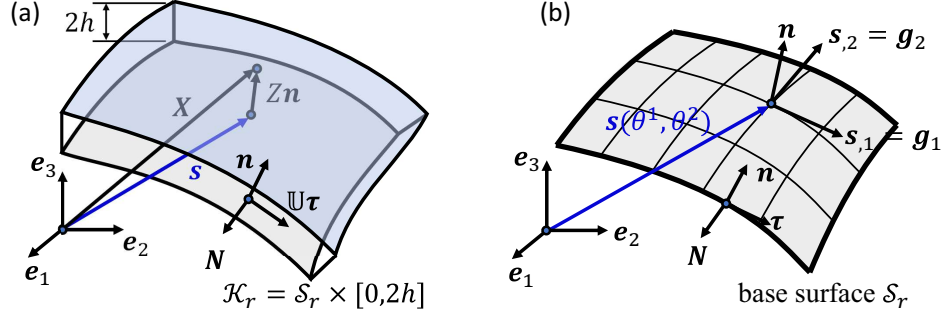$$L_r = b_{11}, \quad M_r = b_{12} = b_{21}, \quad N_r = b_{22}. \tag{3}$$

Figure 1: Position vector in the reference configuration $\mathcal{K}_r$: (a) reference configuration of the shell and decomposition of the position vector $\mathbf{X}$; (b) the curvilinear coordinate system and the local covariant basis on the base surface $\mathcal{S}_r$ of the shell.

As shown in Fig.1a, the position vector $\mathbf{X}$ of a material point in the reference configuration $\mathcal{K}_r$ of the shell can be decomposed into

$$\mathbf{X} = \mathbf{s}(\theta^\alpha) + Z\mathbf{n}(\theta^\alpha), \quad 0 \leq Z \leq 2h, \tag{4}$$

where Z is the coordinate of the point along the normal direction $\mathbf{n}$. Accordingly, the differential of $\mathbf{X}$ yields that

$$d\mathbf{X} = d\mathbf{s} + Zd\mathbf{n} + \mathbf{n}dZ = \mathbf{g}_\alpha d\theta^\alpha + Z\mathbf{n}_{,\alpha} d\theta^\alpha + \mathbf{n}dZ. \tag{5}$$

From the Weingarten equation(Chen, 2017), we have

$$d\mathbf{n} = \mathbf{n}_{,\alpha} d\theta^\alpha = (\mathbf{n}_{,\alpha} \otimes \mathbf{g}^\alpha) \mathbf{g}_\beta d\theta^\beta = -\mathbb{K} d\mathbf{s}, \tag{6}$$

where $\mathbb{K} = -\mathbf{n}_{,\alpha} \otimes \mathbf{g}^\alpha$ is the curvature tensor. The mean and Gaussian curvatures of the surface $\mathcal{S}_r$ are given by

$$H = \frac{1}{2}\mathrm{tr}\,(\mathbb{K}), \quad K = \mathrm{Det}\,(\mathbb{K}). \tag{7}$$

9

By substituting (6) into (5), we obtain

$$dX = \mathbb{U}ds + \mathbf{n}dZ = \hat{\mathbf{g}}_\alpha d\theta^\alpha + \mathbf{n}dZ, \tag{8}$$

where $\mathbb{U} = \mathbf{g}_\alpha \otimes \mathbf{g}^\alpha - Z\mathbb{K}$ and $\hat{\mathbf{g}}_\alpha = \mathbb{U}\mathbf{g}_\alpha$. We further denote $\hat{\mathbf{g}}^\alpha = \mathbb{U}^{-T}\mathbf{g}^\alpha$, then $\{\hat{\mathbf{g}}_\alpha\}_{\alpha=1,2}$ and $\{\hat{\mathbf{g}}^\alpha\}_{\alpha=1,2}$ form the covariant and contravariant base vectors at an arbitrary point in the shell, which are also orthogonal to $\mathbf{n}$. Notice that the thickness of the shell is much smaller than the radius of curvature of $\mathcal{S}_r$; thus, $\mathbb{U}$ should be an invertible tensor. From (8), the area element on the base surface and the volume element in the shell can be written into

$$dA = |\mathbf{g}_1 \wedge \mathbf{g}_2| \, d\theta^1 d\theta^2 = \sqrt{g_{11}g_{22} - g_{12}^2} \, d\theta^1 d\theta^2,$$
$$dV = \mathrm{Det}(\mathbb{U})dAdZ = \left(1 - 2HZ + KZ^2\right) dAdZ. \tag{9}$$

Regarding area element on the lateral surface da, the local differential follows (8) that

$$\mathbf{N}da = (\mathbb{U}\boldsymbol{\tau}) \times \mathbf{n} \, dsdZ, \tag{10}$$

where $\mathbf{N}$ is the outward normal unit vector of the lateral surface, and $\boldsymbol{\tau}$ is the unit tangent vector along the edge curve $\partial\mathcal{S}_r$ of the base surface, and s is the arc-length variable on the edge curve $\partial\mathcal{S}_r$ of the base surface. The norm of vector $(\mathbb{U}\boldsymbol{\tau}) \times \mathbf{n}$ is denoted by $\sqrt{g_\tau}$ such that $da = \sqrt{g_\tau}dsdZ$.

Due to the growth effect and the external loads, the configuration of the shell will deform from $\mathcal{K}_r$ to the current configuration $\mathcal{K}_t$ in $\mathcal{R}^3$. Within the orthonormal frame $\{O; \mathbf{e}_1, \mathbf{e}_2, \mathbf{e}_3\}$, the position vector of a material point in $\mathcal{K}_t$ is denoted by $\mathbf{x}(\theta^\alpha, Z) = x^i(\theta^\alpha, Z)\mathbf{e}_i$. The deformation gradient tensor $\mathbb{F}$ can then be calculated through

$$\mathbb{F} = \mathbf{x}_{,\alpha} \otimes \hat{\mathbf{g}}^\alpha + \frac{\partial \mathbf{x}}{\partial Z} \otimes \mathbf{n} = (\nabla\mathbf{x})\,\mathbb{U}^{-1} + \frac{\partial \mathbf{x}}{\partial Z} \otimes \mathbf{n}, \tag{11}$$

10

where ∇ is the in-plane 2-D gradient on the base surface $\mathcal{S}_r$ ($\nabla \mathbf{x} = \mathbf{x}_{,\alpha} \otimes \mathbf{g}^\alpha$).

Following the basic assumption of growth mechanics (Kondaurov and Nikitin, 1987; Rodriguez et al., 1994; Ben Amar and Goriely, 2005; Dort-divanlioglu et al., 2017; Mehta et al., 2021; Groh, 2022), the deformation gradient tensor $\mathbb{F}$ is decomposed into

$$\mathbb{F} = \mathbb{A}\mathbb{G}, \tag{12}$$

where $\mathbb{A}$ is the elastic strain tensor and $\mathbb{G}$ is the growth tensor. It is known that the rate of growth is relatively slow compared with the elastic response of the material, thus the distribution of the growth tensor $\mathbb{G}$ in the shell is assumed to be given and does not change.

As the elastic deformations of soft materials (e.g., soft biological tissues, polymeric gels) are generally isochoric, the following constraint equation should be adopted

$$R(\mathbb{F}, \mathbb{G}) = J_G R_0(\mathbb{A}) = J_G \left(\text{Det}(\mathbb{A}) - 1 \right) = 0, \tag{13}$$

where $J_G = \text{Det}(\mathbb{G})$. Furthermore, we suppose the material has an elastic strain-energy function

$$\phi(\mathbb{F}, \mathbb{G}) = J_G \phi_0(\mathbb{A}) = J_G \phi_0(\mathbb{F}\mathbb{G}^{-1}). \tag{14}$$

Then, the nominal stress tensor $\mathbb{S}$ can be calculated through the constitutive equation

$$\mathbb{S} = \frac{\partial \phi}{\partial \mathbb{F}} - p \frac{\partial R}{\partial \mathbb{F}} = J_G \mathbb{G}^{-1} \left(\frac{\partial \phi_0(\mathbb{A})}{\partial \mathbb{A}} - p \frac{\partial R_0(\mathbb{A})}{\partial \mathbb{A}} \right), \tag{15}$$

where $p(\theta^\alpha, Z)$ is the Lagrange multiplier associated with the constraint (13).

During the growing process, the hyperelastic shell satisfies the following mechanical equilibrium equation

$$\text{Div}\,\mathbb{S} = (\mathbb{S}_{,\alpha})^T\,\hat{\mathbf{g}}^\alpha + \left(\frac{\partial \mathbb{S}}{\partial Z}\right)^T \mathbf{n} = \mathbf{0}, \quad \text{in}\;\; \mathcal{S}_r \times [0, 2h]. \tag{16}$$

We suppose that the bottom and top surfaces of the shell are subjected to the applied traction $\mathbf{q}^\pm$, which yields the boundary conditions

$$\mathbb{S}^T\mathbf{n}|_{Z=0} = -\mathbf{q}^-, \quad \mathbb{S}^T\mathbf{n}|_{Z=2h} = \mathbf{q}^+, \quad \text{on}\;\; \mathcal{S}_r. \tag{17}$$

On the lateral surface $\partial\mathcal{S}_r \times [0, 2h]$ of the shell, we suppose the applied traction is $\mathbf{q}(s, Z)$, where s is the arc-length variable of boundary curve $\partial\mathcal{S}_r$. So, we also have the boundary condition

$$\mathbb{S}^T\mathbf{N} = \mathbf{q}(s, Z) \quad \text{on}\;\; \partial\mathcal{S}_r \times [0, 2h]. \tag{18}$$

Eqs. (13) and (16) together with the boundary conditions (17) and (18) constitute the 3D governing system of the shell model, which contains the unknowns $\{\mathbf{x}, p\}$.

2.2. Shell equation system

Starting from the 3D governing system of the shell model, the shell equation system can be derived through a series-expansion and a truncation approach. This approach has been proposed in Dai and Song (2014); Song and Dai (2016); Wang et al. (2016); Li et al. (2019); Yu et al. (2020) for developing the consistent finite-strain plate and shell theories without the growth effect. In Wang et al. (2018); Yu et al. (2022), the finite-strain plate and shell theories of growth have also been established through this approach. For the sake of completeness of the current paper, the key steps of this approach to

12

derive the shell equation system are introduced below (see Yu et al. (2022) for a comprehensive introduction). It should be noted that the derived shell equation system can attain the accuracy of $O(h^2)$. However, to fulfill the requirements of shape-programming in the following sections, we only need to present the shell equation to the asymptotic order of $O(h)$.

To eliminate the thickness variable Z from the 3D governing system, we first conduct the series expansions of the unknowns as follows

$$\mathbf{x}(\theta^\alpha, Z) = \sum_{n=0}^{2} \frac{\mathbf{x}^{(n)}}{n!} Z^n + O\left(Z^3\right), \quad p(\theta^\alpha, Z) = \sum_{n=0}^{2} \frac{p^{(n)}}{n!} Z^n + O\left(Z^3\right),$$
(19)

where $(\cdot)^{(n)} = \partial^n(\cdot)/\left.\partial Z^n\right|_{Z=0}$. According to (19), the deformation gradient tensor $\mathbb{F}$, the elastic strain tensor $\mathbb{A}$ and the nominal stress tensor $\mathbb{S}$ can also be expanded as

$$\mathbb{F} = \mathbb{F}^{(0)} + Z\mathbb{F}^{(1)} + O(Z^2),$$
$$\mathbb{A} = \mathbb{A}^{(0)} + Z\mathbb{A}^{(1)} + O(Z^2),$$
$$\mathbb{S} = \mathbb{S}^{(0)} + Z\mathbb{S}^{(1)} + O(Z^2).$$
(20)

Furthermore, we denote

$$\mathbb{G} = \mathbb{G}^{(0)} + Z\mathbb{G}^{(1)} + O(Z^2),$$
$$\mathbb{G}^{-1} = \bar{\mathbb{G}}^{(0)} + Z\bar{\mathbb{G}}^{(1)} + O(Z^2),$$
$$J_G \mathbb{G}^{-1} = \hat{\mathbb{G}}^{(0)} + Z\hat{\mathbb{G}}^{(1)} + O(Z^2).$$
(21)

Once the growth tensor $\mathbb{G}$ is given, $\bar{\mathbb{G}}^{(n)}$ and $\hat{\mathbb{G}}^{(n)}$ $(n = 0, 1)$ can be calculated directly.

By using the kinematic relations (11) and (12), the concrete expressions of $\mathbb{F}^{(n)}$ and $\mathbb{A}^{(n)}$ $(n = 0, 1)$ in terms of $\mathbf{x}^{(n)}$ $(n = 0, 1, 2)$ can be derived.

13

Further from the constitutive equation (15), we obtain

$$\mathbb{S}^{(0)} = \hat{\mathbb{G}}^{(0)} \left(\mathcal{A}^{(0)} - p^{(0)} \mathcal{R}^{(0)} \right),$$

$$\mathbb{S}^{(1)} = \hat{\mathbb{G}}^{(0)} \left(\mathcal{A}^{(1)} : \mathbb{A}^{(1)} - p^{(0)} \mathcal{R}^{(1)} : \mathbb{A}^{(1)} - p^{(1)} \mathcal{R}^{(0)} \right) + \hat{\mathbb{G}}^{(1)} \left(\mathcal{A}^{(0)} - p^{(0)} \mathcal{R}^{(0)} \right),$$

$$(22)$$

where $\mathcal{A}^{(n)} = \partial^{n+1} \phi_0 / \partial \mathbb{A}^{n+1} |_{\mathbb{A} = \mathbb{A}^{(0)}}$ and $\mathcal{R}^{(n)} = \partial^{n+1} R_0 / \partial \mathbb{A}^{n+1} |_{\mathbb{A} = \mathbb{A}^{(0)}}$ $(n = 0, 1)$.

We substitute (19) and (20) into the constraint equation (13) and the mechanical equilibrium equation (16). The coefficients of Z^n $(n = 0, 1)$ in these equations should be zero, which yield that

$$\text{Det} \left(\mathbb{A}^{(0)} \right) - 1 = 0, \quad \mathcal{R}^{(0)} : \mathbb{A}^{(1)} = 0, \tag{23}$$

and

$$\nabla \cdot \mathbb{S}^{(0)} + \left(\mathbb{S}^{(1)} \right)^T \mathbf{n} = \mathbf{0},$$

$$\nabla \cdot \mathbb{S}^{(1)} + \left(\mathbb{S}^{(2)} \right)^T \mathbf{n} + \mathbb{K}^T \mathbf{g}^\alpha \cdot \mathbb{S}^{(0)}_{,\alpha} = \mathbf{0}. \tag{24}$$

Further substituting (19) and (20) into the boundary conditions (17), another two equations can be obtained

$$\left(\mathbb{S}^{(0)} \right)^T \mathbf{n} = -\mathbf{q}^-,$$

$$\left(\mathbb{S}^{(0)} + 2h \mathbb{S}^{(1)} + 2h^2 \mathbb{S}^{(2)} \right)^T \mathbf{n} = \mathbf{q}^+. \tag{25}$$

Eqs. $(23)_2$ and $(24)_1$ constitute a linear system for $\mathbf{x}^{(2)}$ and $p^{(1)}$. By solving these two equations, we obtain (Yu et al., 2022)

$$\mathbf{x}^{(2)} = \mathbb{D}^{-1} \left(p^{(1)} \mathbf{y} - \mathbf{f} \right), \quad p^{(1)} = \frac{\mathbf{y} \cdot \mathbb{D}^{-1} \mathbf{f} - T}{\mathbf{y} \cdot \mathbb{D}^{-1} \mathbf{y}}, \tag{26}$$

14

where

$$(\mathbb{D})_{ij} = \mathrm{Det}(\mathbb{G}^{(0)}) \left(\mathcal{A}^{(1)} - p^{(0)}\mathcal{R}^{(1)}\right)_{kilj} \left(\left(\bar{\mathbb{G}}^{(0)}\right)^T \mathbf{n}\right)_k \left(\left(\bar{\mathbb{G}}^{(0)}\right)^T \mathbf{n}\right)_l,$$

$$\mathbf{y} = \mathcal{R}^{(0)T}\hat{\mathbb{G}}^{(0)T}\mathbf{n},$$

$$\mathbf{f} = \left[\left(\mathcal{A}^{(1)} - p^{(0)}\mathcal{R}^{(1)}\right) : \left[\mathbb{F}^{(0)}\bar{\mathbb{G}}^{(1)} + \left(\mathbf{x}^{(1)} \otimes \nabla + \mathbf{x}^{(0)} \otimes \mathbb{K}\right)\bar{\mathbb{G}}^{(0)}\right]\right]^T \hat{\mathbb{G}}^{(0)T}\mathbf{n}$$

$$+ \left(\mathcal{A}^{(0)} - p^{(0)}\mathcal{R}^{(0)}\right)^T \hat{\mathbb{G}}^{(1)T}\mathbf{n} + \nabla \cdot \mathbb{S}^{(0)},$$

$$T = \mathrm{Det}(\mathbb{G}^{(0)})\mathcal{R}^{(0)} : \left[\left(\mathbf{x}^{(1)} \otimes \nabla + \mathbf{x}^{(0)} \otimes \nabla\mathbb{K}\right)\bar{\mathbb{G}}^{(0)} + \mathbb{F}^{(0)}\bar{\mathbb{G}}^{(1)}\right].$$

The expressions of $\mathbf{x}^{(1)}$ and $p^{(0)}$ in terms of $\mathbf{x}^{(0)}$ can be obtained by solving the equations $(23)_1$ and $(25)_1$. However, as these two equations are non-linear, the explicit expressions of $\mathbf{x}^{(1)}$ and $p^{(0)}$ can only be presented when a concrete form of the strain-energy function $\phi_0(\mathbb{A})$ is given. If the shell is made of the incompressible neo-Hookean material, the explicit expressions of $\mathbf{x}^{(1)}$ and $p^{(0)}$, as well as the expressions of $\mathbf{x}^{(2)}$ and $p^{(1)}$, can be found in Eqs. (A.3) and (A.4) of Appendix A.

To incorporate the effect of curvature of the shell, the factor $\mathrm{Det}(\mathbb{U})|_{Z=2h} = 1 - 4hH + 4h^2K$ is multiplied onto $(25)_2$ (Song and Dai, 2016). In the remainder of this paper, we assume $H \leq O(1)$ and $K \leq O(1)$, to ensure $1 > |4hH| > |4h^2K|$ such that the terms consisting h^2H and h^2K can be dropped reasonably when the required order of equation is set as $O(h)$. By subtracting $(25)_1$ from $(25)_2$ and dividing it by $2h$, the following equation is obtained (where the terms of order higher than $O(h)$ have been dropped)

$$(1 - 4hH)\left(\mathbb{S}^{(1)}\right)^T \mathbf{n} + h\left(\mathbb{S}^{(2)}\right)^T \mathbf{n} = \frac{(1 - 4hH)\,\mathbf{q}^+ + \mathbf{q}^-}{2h}, \quad \text{on } \mathcal{S}_r. \quad (27)$$

By virtue of the relations given in (24), (27) can be rewritten into 2D vector

15

shell equation

$$(1 - 4hH)\,\nabla\cdot\mathbb{S}^{(0)} + h\left(\nabla\cdot\mathbb{S}^{(1)} + \mathbb{K}^T\mathbf{g}^\alpha\cdot\mathbb{S}^{(0)}_{,\alpha}\right) = -\frac{(1 - 4hH)\,\mathbf{q}^+ + \mathbf{q}^-}{2h}, \quad \text{on } \mathcal{S}_r.$$
(28)

which contains the unknown $\mathbf{x}^{(0)}(\theta^\alpha)$. In fact, $\mathbf{x}^{(0)}(\theta^\alpha)$ provides the parametric equation for the base surface $\mathcal{S}$ in the current configuration of the shell.

To establish a complete shell equation system, the boundary conditions on the edge $\partial\mathcal{S}_r$ should also be proposed. Based on the boundary condition (18) in the 3D governing system, the following edge boundary conditions can be proposed

$$\left(\mathbb{S}^{(0)} + h\mathbb{S}^{(1)}\right)^T \mathbf{N} = \int_0^{2h} \mathbf{q}(s, Z)dZ/(2h) = \bar{\mathbf{q}},$$

$$\int_{\partial\mathcal{S}_r}\int_0^{2h}\left(\mathbb{S}^T\mathbf{N}\right)\wedge(\mathbf{x}(s, Z) - \mathbf{x}(s, h))\sqrt{g_\tau}dZds$$
(29)

$$= \int_{\partial\mathcal{S}_r}\int_0^{2h}\mathbf{q}(s, Z)\wedge(\mathbf{x}(s, Z) - \mathbf{x}(s, h))\sqrt{g_\tau}dZds = \bar{\mathbf{m}},$$

where $\bar{\mathbf{q}}$ and $\bar{\mathbf{m}}$ are the average traction and the bending moment (about the middle surface $Z = h$) applied on the lateral surface of the shell. Eqs. (28) and (29) constitute the shell equation system.

The current shell theory is established within the framework of finite-strain elasticity, which takes the growth effect and the constraint of elastic incompressibility into account. Except some smoothness requirements to conduct series expansions, this shell theory makes no ad hoc assumptions on the displacement or stress components. Thus, this shell theory is adequate for modeling the growth-induced large deformations of thin hyperelastic shells. By incorporating more high-order terms in the series expansions (19), one

16

can derive the shell equation system with the accuracy of $O(h^2)$ (the detailed derivation process can be found in Li et al. (2019) and Yu et al. (2022)). If the growth effect is neglected and some a priori hypotheses are adopted (e.g., the Kirchhoff-Love hypothesis), the current shell theory can also be reduced to some classical shell theories (e.g., the Reissner-Mindlin shell theory) within the small-strain range or some other nonlinear shell (or membrane) theories.

3. Shape-programming of the thin hyperelastic shell

The shell equation system (28)-(29) can be applied to study the growth-induced deformations of the thin hyperelastic shell. For any given growth tensor $\mathbb{G}$ and boundary conditions, once the shell equation system is solved, the obtained solution $\mathbf{x}^{(0)}(\theta^\alpha)$ just represents the base surface $\mathcal{S}$ of the shell in the current configuration $\mathcal{K}_t$. By further using the relations (A.3) and (A.4) given in Appendix A, the 3D configuration of the shell $\mathcal{K}_t$ can also be recovered.

The objective of the current work is to solve an inverse problem. That is, to ensure the shape change of the base surface from $\mathcal{S}_r$ to a certain target shape $\mathcal{S}$, how to arrange the growth tensor (or growth functions) in the shell sample? This problem is referred to as 'shape-programming' of thin hyper-elastic shells (Liu et al., 2016). It should be noted that our goal is not to control the whole 3D configuration of the shell. As the shell equation system (28)-(29) is established on the base surface ($Z = 0$) of the shell, we also focus on the base surface in solving the problem of shape-programming. Different from some previous works of shape-programming through the numerical approach, we aim to derive some explicit analytical formulas that can reveal

17

the relations between the growth functions and the geometrical properties of the base surface clearly. For the purpose of simplicity, we only consider the case that the surfaces of the shell are traction-free, i.e., $\mathbf{q}^{\pm} = \mathbf{q}(s, Z) = \mathbf{0}$ in (28) and (29).
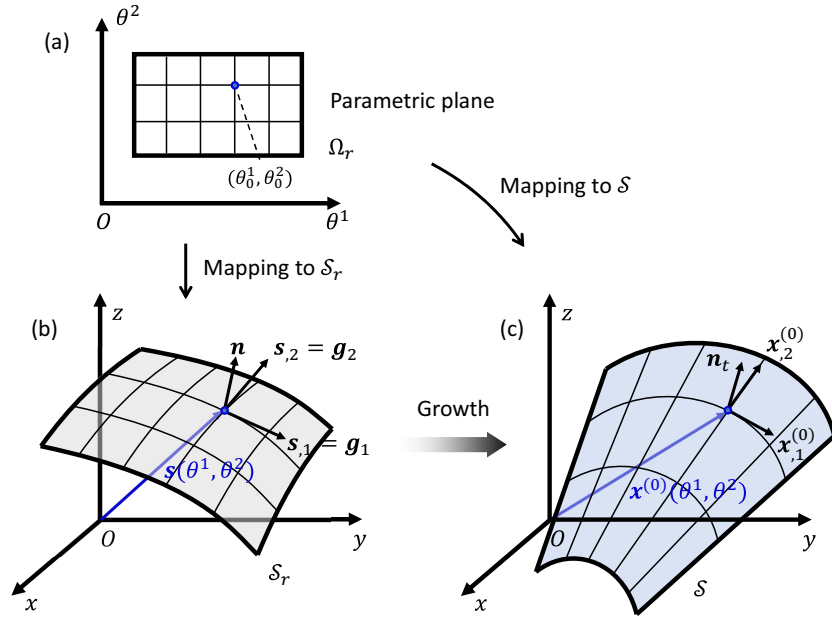

Figure 2: Illustration of the growth process and the mapping from the parametric plane: (a) the variables region Ω_r on the parametric plane $\theta^1\theta^2$; (b) initial base surface $\mathcal{S}_r$; (c) target base surface $\mathcal{S}$.

Suppose the initial and current configurations of the base surface of the shell have the following parametric equations (as shown in Fig. 2):

$$\mathcal{S}_r : \mathbf{s}(\theta^{\alpha}) = \left\{ X^1(\theta^{\alpha}), X^2(\theta^{\alpha}), X^3(\theta^{\alpha}) \right\}, \quad (\theta^{\alpha}) \in \Omega_r, \tag{30}$$

and

$$\mathcal{S} : \mathbf{x}^{(0)}(\theta^{\alpha}) = \left\{ x^1(\theta^{\alpha}), x^2(\theta^{\alpha}), x^3(\theta^{\alpha}) \right\}, \quad (\theta^{\alpha}) \in \Omega_r. \tag{31}$$

18

Eqs. (30) and (31) can be viewed as two continuous mappings from the 2D region Ω_r to $\mathcal{S}_r$ and $\mathcal{S}$, respectively. By fixing one of the variables θ^1 or θ^2, variation of the the other variable can generate the coordinate curves on the surfaces. All of these curves constitute the parametric curves net on $\mathcal{S}_r$ and $\mathcal{S}$. It has been introduced that on the initial configuration $\mathcal{S}_r$, the tangent vectors along the coordinate curves are $\mathbf{s}_{,\alpha} = \mathbf{g}_\alpha = \partial \mathbf{s}/\partial \theta^\alpha$ and unit normal vector is $\mathbf{n} = (\mathbf{g}_1 \wedge \mathbf{g}_2)/\left|\mathbf{g}_1 \wedge \mathbf{g}_2\right|$. Similarly, on base surface $\mathcal{S}$ in the current configuration, the tangent vectors along the coordinate curves are $\mathbf{x}_{,\alpha}^{(0)} = \partial \mathbf{x}^{(0)}/\partial \theta^\alpha$, and the unit normal vector is denoted by $\mathbf{n}_t = (\mathbf{x}_{,1}^{(0)} \wedge \mathbf{x}_{,2}^{(0)})/\left|\mathbf{x}_{,1}^{(0)} \wedge \mathbf{x}_{,2}^{(0)}\right|$ (cf. Fig. 2). If $\mathcal{S}_r$ and $\mathcal{S}$ are regular surfaces, we always have $\mathbf{g}_1 \wedge \mathbf{g}_2 \neq 0$ and $x_{,1}^{(0)} \wedge \mathbf{x}_{,2}^{(0)} \neq 0$. Thus, the normal vector fields are well-defined on $\mathcal{S}_r$ and $\mathcal{S}$.

To facilitate the following derivations, we assume that the parametric curves net generated by $\{\theta^\alpha\}$ is an orthogonal net of curvature lines on $\mathcal{S}_r$. This assumption means that the tangent vectors $\mathbf{g}_1$ and $\mathbf{g}_2$ are perpendicular to each other (i.e., $\mathbf{g}_1 \cdot \mathbf{g}_2 = 0$) and they direct along the two principal directions at any point on $\mathcal{S}_r$. It is known that on a regular surface, such an orthogonal net always exists in the neighbour region of a non-umbilic point (Chen, 2017; Toponogov, 2006). Due to this assumption, some geometrical quantities defined in section 2.1 can be simplified into

$$
\begin{aligned}
&F_r = g_{12} = g_{21} = 0, \quad M_r = b_{12} = b_{21} = 0, \\
&\mathbb{K} = -\mathbf{n}_\alpha \otimes \mathbf{g}^\alpha = \kappa_1 \mathbf{g}_1 \otimes \mathbf{g}^1 + \kappa_2 \mathbf{g}_2 \otimes \mathbf{g}^2, \\
&H = \frac{1}{2}(\kappa_1 + \kappa_2), \quad K = \kappa_1 \kappa_2, \\
&\mathbb{U} = \mathbb{I}_2 - Z\mathbb{K} = (1 - \kappa_1 Z)\mathbf{g}_1 \otimes \mathbf{g}^1 + (1 - \kappa_2 Z)\mathbf{g}_2 \otimes \mathbf{g}^2,
\end{aligned}
\tag{32}
$$

where κ_1 and κ_2 are called the principal curvatures.

19

With the above preparations, we begin to solve the problem of shape-programming of the thin hyperelastic shell. The major task is to reveal the relations between the growth tensor (or growth functions) and the geometrical properties of the target surface $\mathcal{S}$. In general, the solution of shape-programming through differential growth may not be unique, i.e., the same target shape of the shell may be generated from different growth fields (Wang et al., 2019b). In the current work, we focus on the case that the shell attains the stress-free state in the current configuration $\mathcal{K}_t$, i.e., all the components in $\mathbb{S}^{(0)}$ and $\mathbb{S}^{(1)}$ are zero. It is clear that in the stress-free condition, the shell equation system (28) and (29) is satisfied automatically.

Remarks:

- For any given target surface $\mathcal{S}$, one may set different kinds of growth fields in the shell such that the base surface of the shell can attain $\mathcal{S}$ through differential growth. In fact, most of these growth fields will induce the distributions of residual stresses in the shell sample. In the current work, we do not aim to find all of the possible growth fields that can generate the target surface $\mathcal{S}$ (which would be a very difficult task). For simplicity, we only consider the stress-free condition of the shell and try to find one of the possible growth fields such that the target surface $\mathcal{S}$ can be achieved through differential growth.

- Under the assumption of stress free of the shell, the problem of shape-programming becomes easier to be solved. It will be shown that for any given target surface $\mathcal{S}$, we can solve the problem of shape-programming under the stress-free condition and derive the explicit expression of the corresponding growth tensor. Although the stress-free state is only

a specific state of the shell, it has important meaning for engineering applications. For example, the elastic energy of the shell sample attains the minimum value in the stress-free state, which implies that the shell sample is stable in this state. Thus, the obtained results can be utilized for designing intelligent soft devices in the engineering fields.

3.1. Growth tensor in a special case

To analyze the relations between the growth tensor (or growth functions) and the geometrical properties of the target surface $\mathcal{S}$, we first assume that the coordinate curves of $\{\theta^\alpha\}$ also generate a net of curvature lines on the base surface $\mathcal{S}$ in the current configuration. In this special case, the following specific form of the growth tensor will be adopted

$$
\begin{aligned}
\mathbb{G} &= \mathbb{G}^{(0)} + Z\mathbb{G}^{(1)}, \\
\mathbb{G}^{(0)} &= \frac{\lambda_1^{(0)}}{\sqrt{E_r}}\mathbf{g}_1 \otimes \mathbf{g}^1 + \frac{\lambda_2^{(0)}}{\sqrt{G_r}}\mathbf{g}_2 \otimes \mathbf{g}^2 + \mathbf{n} \otimes \mathbf{n}, \\
\mathbb{G}^{(1)} &= \frac{\lambda_1^{(1)}}{\sqrt{E_r}}\mathbf{g}_1 \otimes \mathbf{g}^1 + \frac{\lambda_2^{(1)}}{\sqrt{G_r}}\mathbf{g}_2 \otimes \mathbf{g}^2,
\end{aligned}
\tag{33}
$$

where $\lambda_1^{(0)}$, $\lambda_2^{(0)}$, $\lambda_1^{(1)}$ and $\lambda_2^{(1)}$ are the growth functions to be determined. By substituting (32) and (33) into the kinematic relations (11) and (12), the following expression of the elastic strain tensor $\mathbb{A} = \mathbb{F}\mathbb{G}^{-1}$ can be obtained

$$
\begin{aligned}
\mathbb{A} =&\frac{\sqrt{E_r}}{(1 - \kappa_1 Z)(\lambda_1^{(0)} + Z\lambda_1^{(1)})}\mathbf{x}_{,1} \otimes \mathbf{g}^1 \\
&+ \frac{\sqrt{G_r}}{(1 - \kappa_2 Z)(\lambda_2^{(0)} + Z\lambda_2^{(1)})}\mathbf{x}_{,2} \otimes \mathbf{g}^2 + \frac{\partial \mathbf{x}}{\partial Z} \otimes \mathbf{n},
\end{aligned}
\tag{34}
$$

21

The right Cauchy-Green strain tensor $\mathbb{C} = \mathbb{A}^T\mathbb{A}$ is then given by

$$
\begin{aligned}
\mathbb{C} =& \frac{\mathbf{x}_{,1} \cdot \mathbf{x}_{,1}}{(1 - \kappa_1 Z)^2(\lambda_1^{(0)} + Z\lambda_1^{(1)})^2}\hat{\mathbf{g}}^1 \otimes \hat{\mathbf{g}}^1 + \frac{\mathbf{x}_{,2} \cdot \mathbf{x}_{,2}}{(1 - \kappa_2 Z)^2(\lambda_2^{(0)} + Z\lambda_2^{(1)})^2}\hat{\mathbf{g}}^2 \otimes \hat{\mathbf{g}}^2 \\
&+ \frac{\mathbf{x}_{,1} \cdot \mathbf{x}_{,2}}{(1 - \kappa_1 Z)(1 - \kappa_2 Z)(\lambda_1^{(0)} + Z\lambda_1^{(1)})(\lambda_2^{(0)} + Z\lambda_2^{(1)})}\left(\hat{\mathbf{g}}^1 \otimes \hat{\mathbf{g}}^2 + \hat{\mathbf{g}}^2 \otimes \hat{\mathbf{g}}^1\right) \\
&+ \frac{\mathbf{x}_{,1} \cdot \mathbf{x}_{,Z}}{(1 - \kappa_1 Z)(\lambda_1^{(0)} + Z\lambda_1^{(1)})}\left(\mathbf{n} \otimes \hat{\mathbf{g}}^1 + \hat{\mathbf{g}}^1 \otimes \mathbf{n}\right) \\
&+ \frac{\mathbf{x}_{,2} \cdot \mathbf{x}_{,Z}}{(1 - \kappa_2 Z)(\lambda_2^{(0)} + Z\lambda_2^{(1)})}\left(\mathbf{n} \otimes \hat{\mathbf{g}}^2 + \hat{\mathbf{g}}^2 \otimes \mathbf{n}\right) + (\mathbf{x}_{,Z} \cdot \mathbf{x}_{,Z})\,\mathbf{n} \otimes \mathbf{n},
\end{aligned}
$$
(35)

where $\hat{\mathbf{g}}^1 = \sqrt{E_r}\mathbf{g}^1$ and $\hat{\mathbf{g}}^2 = \sqrt{G_r}\mathbf{g}^2$ are two unit vectors. By substituting $(19)_1$ into (35) and conducting the series expansion of $\mathbb{C}$ with respect to Z, we have the following coefficients of Z^0 and Z^1

$$
\begin{aligned}
\mathbb{C}^{(0)} =& \frac{\mathbf{x}_{,1}^{(0)} \cdot \mathbf{x}_{,1}^{(0)}}{\lambda_1^{(0)2}}\hat{\mathbf{g}}^1 \otimes \hat{\mathbf{g}}^1 + \frac{\mathbf{x}_{,2}^{(0)} \cdot \mathbf{x}_{,2}^{(0)}}{\lambda_2^{(0)2}}\hat{\mathbf{g}}^2 \otimes \hat{\mathbf{g}}^2 + \left(\mathbf{x}^{(1)} \cdot \mathbf{x}^{(1)}\right)\mathbf{n} \otimes \mathbf{n} \\
&+ \frac{\mathbf{x}_{,1}^{(0)} \cdot \mathbf{x}^{(1)}}{\lambda_1^{(0)}}\left(\hat{\mathbf{g}}^1 \otimes \mathbf{n} + \mathbf{n} \otimes \hat{\mathbf{g}}^1\right) + \frac{\mathbf{x}_{,2}^{(0)} \cdot \mathbf{x}^{(1)}}{\lambda_2^{(0)}}\left(\hat{\mathbf{g}}^2 \otimes \mathbf{n} + \mathbf{n} \otimes \hat{\mathbf{g}}^2\right),
\end{aligned}
$$
(36)

$$
\begin{aligned}
\mathbb{C}^{(1)} =& \frac{2}{\lambda_1^{(0)2}}\left[\mathbf{x}_{,1}^{(0)} \cdot \mathbf{x}_{,1}^{(1)} + \left(\kappa_1 - \frac{\lambda_1^{(1)}}{\lambda_1^{(0)}}\right)\mathbf{x}_{,1}^{(0)} \cdot \mathbf{x}_{,1}^{(0)}\right]\hat{\mathbf{g}}^1 \otimes \hat{\mathbf{g}}^1 \\
&+ \frac{2}{\lambda_2^{(0)2}}\left[\mathbf{x}_{,2}^{(0)} \cdot \mathbf{x}_{,2}^{(1)} + \left(\kappa_2 - \frac{\lambda_2^{(1)}}{\lambda_2^{(0)}}\right)\mathbf{x}_{,2}^{(0)} \cdot \mathbf{x}_{,2}^{(0)}\right]\hat{\mathbf{g}}^2 \otimes \hat{\mathbf{g}}^2 \\
&+ \left(2\mathbf{x}^{(1)} \cdot \mathbf{x}^{(2)}\right)\mathbf{n} \otimes \mathbf{n} + \frac{\mathbf{x}_{,2}^{(0)} \cdot \mathbf{x}_{,1}^{(1)} + \mathbf{x}_{,1}^{(0)} \cdot \mathbf{x}_{,2}^{(1)}}{\lambda_1^{(0)}\lambda_2^{(0)}}\left(\hat{\mathbf{g}}^1 \otimes \hat{\mathbf{g}}^2 + \hat{\mathbf{g}}^2 \otimes \hat{\mathbf{g}}^1\right) \\
&+ \left[\frac{\mathbf{x}_{,1}^{(1)} \cdot \mathbf{x}^{(1)} + \mathbf{x}_{,1}^{(0)} \cdot \mathbf{x}^{(2)}}{\lambda_1^{(0)}} + \frac{\mathbf{x}_{,1}^{(0)} \cdot \mathbf{x}^{(1)}}{\lambda_1^{(0)}}\left(\kappa_1 - \frac{\lambda_1^{(1)}}{\lambda_1^{(0)}}\right)\right]\left(\hat{\mathbf{g}}^1 \otimes \mathbf{n} + \mathbf{n} \otimes \hat{\mathbf{g}}^1\right) \\
&+ \left[\frac{\mathbf{x}_{,2}^{(1)} \cdot \mathbf{x}^{(1)} + \mathbf{x}_{,2}^{(0)} \cdot \mathbf{x}^{(2)}}{\lambda_2^{(0)}} + \frac{\mathbf{x}_{,2}^{(0)} \cdot \mathbf{x}^{(1)}}{\lambda_2^{(0)}}\left(\kappa_2 - \frac{\lambda_2^{(1)}}{\lambda_2^{(0)}}\right)\right]\left(\hat{\mathbf{g}}^2 \otimes \mathbf{n} + \mathbf{n} \otimes \hat{\mathbf{g}}^2\right),
\end{aligned}
$$
(37)

For isotropic incompressible hyperelastic material, it is known that the elastic strain-energy function only depends on the two invariants I_1 and I_2 of $\mathbb{C}$, i.e., $\phi_0(\mathbb{A}) = \phi_0(I_1, I_2)$. Based on this constitutive form of ϕ_0, the nominal stress tensor $\mathbb{S}$ given in (15) can be rewritten into

$$
\begin{aligned}
\mathbb{S} &= J_G \mathbb{G}^{-1} \left[\frac{\partial \phi_0}{\partial I_1} \frac{\partial I_1}{\partial \mathbb{A}} + \frac{\partial \phi_0}{\partial I_2} \frac{\partial I_2}{\partial \mathbb{A}} - p \mathbb{A}^{-1} \right] \\
&= J_G \mathbb{G}^{-1} \left[2 \frac{\partial \phi_0}{\partial I_1} \mathbb{A}^T + 2 \frac{\partial \phi_0}{\partial I_2} \left(I_1 \mathbb{I} - \mathbb{C} \right) \mathbb{A}^T - p \mathbb{A}^{-1} \right],
\end{aligned}
\tag{38}
$$

where the relations $\partial I_1 / \partial \mathbb{A} = 2 \mathbb{A}^T$ and $\partial I_2 / \partial \mathbb{A} = 2(I_1 \mathbb{I} - \mathbb{C}) \mathbb{A}^T$ have been used. We denote

$$
\mathbb{A}^{-1} = \bar{\mathbb{A}}^{(0)} + Z \bar{\mathbb{A}}^{(1)} + O(Z^2),
$$

$$
\mathbb{C} = \mathbb{C}^{(0)} + Z \mathbb{C}^{(1)} + O(Z^2), \quad I_1 = I_1^{(0)} + Z I_1^{(1)} + O(Z^2), \tag{39}
$$

$$
\frac{\partial \phi_0}{\partial I_1} = d_1^{(0)} + Z d_1^{(1)} + O(Z^2), \quad \frac{\partial \phi_0}{\partial I_2} = d_2^{(0)} + Z d_2^{(1)} + O(Z^2),
$$

Then, the following expressions of $\mathbb{S}^{(0)}$ and $\mathbb{S}^{(1)}$ can be derived from (38)

$$
\begin{aligned}
\mathbb{S}^{(0)} &= \hat{\mathbb{G}}^{(0)} \left\{ 2 \left[d_1^{(0)} + d_2^{(0)} \left(I_1^{(0)} \mathbb{I} - \mathbb{C}^{(0)} \right) \right] \left(\mathbb{A}^{(0)} \right)^T - p^{(0)} \bar{\mathbb{A}}^{(0)} \right\}, \\
\mathbb{S}^{(1)} &= \hat{\mathbb{G}}^{(0)} \left\{ 2 \left[d_1^{(0)} + d_2^{(0)} \left(I_1^{(0)} \mathbb{I} - \mathbb{C}^{(0)} \right) \right] \left(\mathbb{A}^{(1)} \right)^T \right\} \\
&\quad + \hat{\mathbb{G}}^{(0)} \left\{ 2 \left[d_1^{(1)} + d_2^{(1)} \left(I_1^{(0)} \mathbb{I} - \mathbb{C}^{(0)} \right) + d_2^{(0)} \left(I_1^{(1)} \mathbb{I} - \mathbb{C}^{(1)} \right) \right] \left(\mathbb{A}^{(0)} \right)^T \right\} \\
&\quad + \hat{\mathbb{G}}^{(0)} \left(-p^{(0)} \bar{\mathbb{A}}^{(1)} - p^{(1)} \bar{\mathbb{A}}^{(0)} \right).
\end{aligned}
\tag{40}
$$

To ensure $\mathbb{S}^{(0)}$ and $\mathbb{S}^{(1)}$ to be zero tensors, one sufficient condition is that

$$
\mathbb{C}^{(0)} = \mathbb{I}, \quad \mathbb{C}^{(1)} = \mathbf{0}, \quad p^{(0)} = 2 \left(d_1^{(0)} + 2 d_2^{(0)} \right), \quad p^{(1)} = 2 \left(d_1^{(1)} + 2 d_2^{(1)} \right).
\tag{41}
$$

From $(41)_1$ and $(41)_2$, the growth functions $\{\lambda_\alpha^{(0)}\}$ and $\{\lambda_\alpha^{(1)}\}$ can be easily determined. In fact, by substituting (36) into $(41)_1$, we obtain

$$
\lambda_1^{(0)} = \sqrt{E}, \quad \lambda_2^{(0)} = \sqrt{G}, \tag{42}
$$

23

where $E = \mathbf{x}_{,1}^{(0)} \cdot \mathbf{x}_{,1}^{(0)}$ and $G = \mathbf{x}_{,2}^{(0)} \cdot \mathbf{x}_{,2}^{(0)}$ are two of the first fundamental quantities of surface $\mathcal{S}$. As we assume the coordinate curves of $\{\theta^\alpha\}$ generate a net of curvature lines on $\mathcal{S}$, another first fundamental quantity $F = \mathbf{x}_{,1}^{(0)} \cdot \mathbf{x}_{,2}^{(0)} = 0$. Further from the relation $(41)_1$, we have

$$\mathbf{x}_{,1}^{(0)} \cdot \mathbf{x}^{(1)} = 0, \quad \mathbf{x}_{,2}^{(0)} \cdot \mathbf{x}^{(1)} = 0, \quad \mathbf{x}^{(1)} \cdot \mathbf{x}^{(1)} = 1,$$

$$\Rightarrow \mathbf{x}^{(1)} = \frac{\mathbf{x}_{,1}^{(0)} \wedge \mathbf{x}_{,2}^{(0)}}{\left| \mathbf{x}_{,1}^{(0)} \wedge \mathbf{x}_{,2}^{(0)} \right|} = \mathbf{n}_t. \tag{43}$$

By substituting (42) and (43) into (37), then from $(41)_2$, we obtain

$$\lambda_1^{(1)} = \left(\kappa_1 - \frac{L}{E} \right) \sqrt{E}, \quad \lambda_2^{(1)} = \left(\kappa_2 - \frac{N}{G} \right) \sqrt{G}, \tag{44}$$

where $L = -\mathbf{x}_{,1}^{(0)} \cdot \mathbf{n}_{t,1}$ and $N = -\mathbf{x}_{,2}^{(0)} \cdot \mathbf{n}_{t,2}$ are two of the second fundamental quantities of surface $\mathcal{S}$. Another second fundamental quantity $M = -\mathbf{x}_{,1}^{(0)} \cdot \mathbf{n}_{t,2} = -\mathbf{x}_{,2}^{(0)} \cdot \mathbf{n}_{t,1} = 0$ due to the net of curvature lines on $\mathcal{S}$. To ensure all the components of $\mathbb{C}^{(1)}$ to be zero, we also need to set $\mathbf{x}^{(2)} = \mathbf{0}$. By substituting (42) and (44) into (33), we obtain

$$\mathbb{G} = \left[1 + Z \left(\kappa_1 - \frac{L}{E} \right) \right] \sqrt{\frac{E}{E_r}} \mathbf{g}_1 \otimes \mathbf{g}^1$$
$$+ \left[1 + Z \left(\kappa_2 - \frac{N}{G} \right) \right] \sqrt{\frac{G}{G_r}} \mathbf{g}_2 \otimes \mathbf{g}^2 + \mathbf{n} \otimes \mathbf{n}, \tag{45}$$

which is just the growth tensor that can result in the shape change of the base surface of the shell from $\mathcal{S}_r$ to $\mathcal{S}_t$ in the special case (i.e., the coordinate curves of $\{\theta^\alpha\}$ generate a net of curvature lines on $\mathcal{S}$).

The growth functions $\lambda_1^{(0)}$ and $\lambda_2^{(0)}$ given in (42) have the same expressions as those obtained from the plate model (where the incompressible Neo-Hookean material is taken into account) (Wang et al., 2022). In fact, $\lambda_1^{(0)}$

24

and $\lambda_2^{(0)}$ just represent the extension or shrinkage of the material along the coordinate curves of $\{\theta^\alpha\}$ on $\mathcal{S}_r$. The growth functions $\lambda_1^{(1)}$ and $\lambda_2^{(1)}$ given in (44) involve the principal curvatures κ_1 and κ_2 of $\mathcal{S}_r$, which are different from the results of the plate model (Wang et al., 2022). It should be noted that the growth functions given in (42) and (44) are independent of the strain-energy function ϕ_0, which should be valid for different kinds of hyperelastic shells. If the shell is made of incompressible neo-Hookean material, the results (42) and (44) can be derived through another approach, which is introduced in Appendix A.

It should be noted that the growth tensor $\mathbb{G}$ considered in this section has a diagonal form (cf. Eqs. (33) and (45)). Compared with the growth tensor with a general form, the diagonal growth tensor is easier to be generated in the shell sample. For examples, one can put two sets of fibres along the curvature lines of surface $\mathcal{S}_r$. Then, the growth tensor with the diagonal form can be realized through the elongation or shortening of the fibres according to the growth functions given in (42) and (43) (the growth functions change linearly along the thickness direction of the shell).

3.2. Growth tensor in general cases

The formulas (42) and (44) are derived based on the assumption that the coordinate curves of variables $\{\theta^\alpha\}$ constitute an orthogonal net of curvature lines in the current configuration of the base surface $\mathcal{S}$. Generally, this assumption cannot be satisfied by the parametric equation $\mathbf{x}^{(0)}(\theta^\alpha)$. To tackle the problem in general cases, some further manipulations are required.

3.2.1. Change of the parametric variables

First, to generate a net of curvature lines on the surface $\mathcal{S}$, we consider the following change of variables

$$\theta^1 = \theta^1\left(\eta^1, \eta^2\right), \quad \theta^2 = \theta^2\left(\eta^1, \eta^2\right),\tag{46}$$

where $\theta^1\left(\eta^1, \eta^2\right)$ and $\theta^2\left(\eta^1, \eta^2\right)$ are supposed to be sufficient smooth and the Jacobi determinant $\partial(\theta^1, \theta^2)/\partial(\eta^1, \eta^2) > 0$. The transformation (46) defines a bijection between the planar parametric region Ω_r in the $\theta^1\theta^2$-plane and the planar parametric region Ω_r^* in the $\eta^1\eta^2$-plane (cf. Fig. 3).
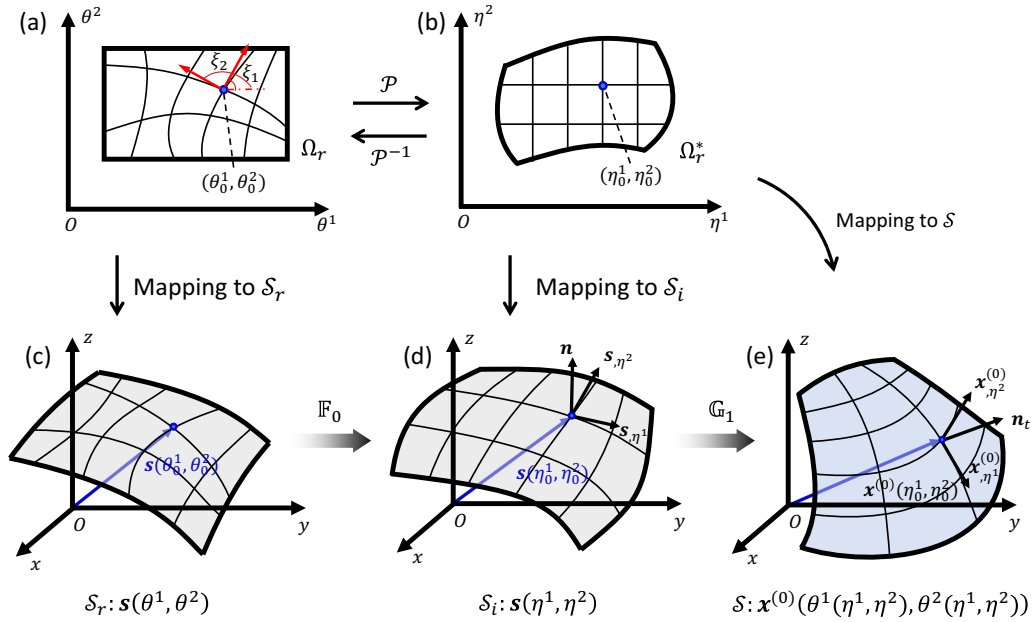
Figure 3: Bijection between the region Ω_r and Ω_r^*, and the decomposition of the growth process: (a) the original region Ω_r on the parametric plane $\theta^1\theta^2$; (b) the new region Ω_r^* on the parametric plane $\eta^1\eta^2$; (c) the base surface $\mathcal{S}_r$ in the referential configuration $\mathcal{K}_r$; (d) the base surface $\mathcal{S}_i$ in the intermediate configuration $\mathcal{K}_i$; (e) the target base surface $\mathcal{S}$ in the current configuration $\mathcal{K}_t$.

26

Through the change of variables, the surface $\mathcal{S}$ has a new parametric equation $\mathbf{x}^*(\eta^1, \eta^2) = \mathbf{x}^{(0)}\left(\theta^1\left(\eta^1, \eta^2\right), \theta^2\left(\eta^1, \eta^2\right)\right)$. The first-order derivatives of $\mathbf{x}^*(\eta^1, \eta^2)$ are given by

$$
\begin{aligned}
\mathbf{x}^*_{,\eta^1} = \mathbf{x}^*_{,\theta^1}\frac{\partial\theta^1}{\partial\eta^1} + \mathbf{x}^*_{,\theta^2}\frac{\partial\theta^2}{\partial\eta^1} = A_1\left(\mathbf{x}^*_{,\theta^1}\cos\xi_1 + \mathbf{x}^*_{,\theta^2}\sin\xi_1\right), \\
\mathbf{x}^*_{,\eta^2} = \mathbf{x}^*_{,\theta^1}\frac{\partial\theta^1}{\partial\eta^2} + \mathbf{x}^*_{,\theta^2}\frac{\partial\theta^2}{\partial\eta^2} = A_2\left(\mathbf{x}^*_{,\theta^1}\cos\xi_2 + \mathbf{x}^*_{,\theta^2}\sin\xi_2\right),
\end{aligned}
\tag{47}
$$

where

$$
\begin{aligned}
A_1 = \sqrt{\left(\frac{\partial\theta^1}{\partial\eta^1}\right)^2 + \left(\frac{\partial\theta^2}{\partial\eta^1}\right)^2}, \quad \cos\xi_1 = \frac{1}{A_1}\frac{\partial\theta^1}{\partial\eta^1}, \quad \sin\xi_1 = \frac{1}{A_1}\frac{\partial\theta^2}{\partial\eta^1}, \\
A_2 = \sqrt{\left(\frac{\partial\theta^1}{\partial\eta^2}\right)^2 + \left(\frac{\partial\theta^2}{\partial\eta^2}\right)^2}, \quad \cos\xi_2 = \frac{1}{A_2}\frac{\partial\theta^1}{\partial\eta^2}, \quad \sin\xi_2 = \frac{1}{A_2}\frac{\partial\theta^2}{\partial\eta^2}.
\end{aligned}
\tag{48}
$$

To ensure that the new coordinate curves (i.e., the η^1- and η^2-curves on $\mathcal{S}$) constitute an orthogonal net of curvature lines, $\mathbf{x}^*_{,\eta^1}$ and $\mathbf{x}^*_{,\eta^2}$ should be aligned with the principal directions at any point on $\mathcal{S}$, which requires that the following equation is satisfied (Toponogov, 2006; Chen, 2017)

$$
(LF - ME)\cos^2\xi + (LG - NE)\cos\xi\sin\xi + (MG - NF)\sin^2\xi = 0, \tag{49}
$$

where $\{E, F, G\}$ and $\{L, M, N\}$ are the first and second fundamental quantities of the surface $\mathcal{S}$ calculated from the original parametric equation $\mathbf{x}^{(0)}(\theta^\alpha)$. On the other hand, as the Jacobi determinant $\partial(\theta^1, \theta^2)/\partial(\eta^1, \eta^2) > 0$, we have the inverse Jacobi matrix

$$
\begin{pmatrix} \frac{\partial\eta^1}{\partial\theta^1} & \frac{\partial\eta^2}{\partial\theta^1} \\ \frac{\partial\eta^1}{\partial\theta^2} & \frac{\partial\eta^2}{\partial\theta^2} \end{pmatrix} = \begin{pmatrix} \frac{\partial\theta^1}{\partial\eta^1} & \frac{\partial\theta^1}{\partial\eta^2} \\ \frac{\partial\theta^2}{\partial\eta^1} & \frac{\partial\theta^2}{\partial\eta^2} \end{pmatrix}^{-1}. \tag{50}
$$

By virtue of (50), the differential forms $d\eta^1$ and $d\eta^2$ can be written into

$$
\begin{aligned}
d\eta^1 = \frac{\partial\eta^1}{\partial\theta^1}d\theta^1 + \frac{\partial\eta^1}{\partial\theta^2}d\theta^2 = A_1^*\left(\sin\xi_2 d\theta^1 - \cos\xi_2 d\theta^2\right), \\
d\eta^2 = \frac{\partial\eta^2}{\partial\theta^1}d\theta^1 + \frac{\partial\eta^2}{\partial\theta^2}d\theta^2 = A_2^*\left(\cos\xi_1 d\theta^2 - \sin\xi_1 d\theta^1\right),
\end{aligned}
\tag{51}
$$

where

$$A_1^* = \frac{1}{A_1 \left(\cos \xi_1 \sin \xi_2 - \sin \xi_1 \cos \xi_2 \right)}, \quad A_2^* = \frac{1}{A_2 \left(\cos \xi_1 \sin \xi_2 - \sin \xi_1 \cos \xi_2 \right)}. \tag{52}$$

To make the differential forms $d\eta^1$ and $d\eta^2$ given in (51) to be integrable, it necessary to derive the explicit expressions of the transformation between $\{\theta^1, \theta^2\}$ and $\{\eta^1, \eta^2\}$. To our knowledge, there are still no universal formulas that can be used to determine the integrating factors for any differential forms (Chen, 2017). In some particular situations, the integrating factors can be obtained by adopting appropriate methods. Once the integrating factors are found, the explicit expressions of $\eta^1(\theta^1, \theta^2)$ and $\eta^2(\theta^1, \theta^2)$ can be obtained by the first integrals of the differential forms (51). Accordingly, the expressions of $\theta^1(\eta^1, \eta^2)$ and $\theta^2(\eta^1, \eta^2)$ are also obtained.

On the parametric variable region Ω_r^* in the $\eta^1\eta^2$-plane, we define a new surface $\mathcal{S}_i$ in $\mathcal{R}^3$, which has the following parametric equation

$$\mathcal{S}_i: \ \mathbf{s}(\eta^\alpha) = \left\{ X^1(\eta^\alpha), X^2(\eta^\alpha), X^3(\eta^\alpha) \right\}, \quad (\eta^\alpha) \in \Omega_r^*. \tag{53}$$

Notice that $\mathcal{S}_i$ and $\mathcal{S}_r$ have the same parametric equation, but they are defined on the different parametric variable regions. In fact, $\mathcal{S}_i$ and $\mathcal{S}_r$ should be the different subregions contained in a larger surface. According to the assumption on the parametric equation $\mathbf{s}(\eta^\alpha)$, the coordinate curves of $\{\eta^\alpha\}$ constitute a net of curvature lines on $\mathcal{S}_i$. By virtue of the variable change $\eta^1(\theta^1, \theta^2)$ and $\eta^2(\theta^1, \theta^2)$, another parametric equation of surface $\mathcal{S}_i$ can be obtained as follow

$$\mathcal{S}_i: \ \mathbf{s}^*(\theta^\alpha) = \mathbf{s}(\eta^1(\theta^1, \theta^2), \eta^2(\theta^1, \theta^2)), \quad (\theta^\alpha) \in \Omega_r, \tag{54}$$

28

which is defined on the parametric variable region Ω_r in the $\theta^1\theta^2$-plane. We choose $\mathcal{S}_i$ as the shape of the base surface of the shell in an intermediate configuration $\mathcal{K}_i$. The position vector $\mathbf{X}^*$ of a material point in $\mathcal{K}_i$ is set to be (cf. Eq. (4))

$$
\begin{aligned}
\mathbf{X}^* &= \mathbf{s}^*(\theta^\alpha) + Z\mathbf{n}^*(\theta^\alpha), \\
&= \mathbf{s}(\eta^1(\theta^\alpha), \eta^2(\theta^\alpha)) + Z\mathbf{n}(\eta^1(\theta^\alpha), \eta^2(\theta^\alpha)), \quad (\theta^\alpha) \in \Omega_r, \ 0 \le Z \le 2h.
\end{aligned}
\tag{55}
$$

3.2.2. The two-step deformation process

Based on the above results, we can write out the growth tensor that produces the shape change of the base surface of the shell from $\mathcal{S}_r$ to $\mathcal{S}$. As shown in Fig. 3, the whole deformation process is divided into two steps. In the first step, we consider the deformation of the shell from the reference configuration $\mathcal{K}_r$ to the intermediate configuration $\mathcal{K}_i$ (i.e., the shape change of the base surface from $\mathcal{S}_r$ to $\mathcal{S}_i$). Based on (54) and (55), it is known that the corresponding deformation gradient tensor should be given by

$$
\begin{aligned}
\mathbb{F}_0 &= (\nabla\mathbf{X}^*)\mathbb{U}^{-1} + \frac{\partial\mathbf{X}^*}{\partial Z} \otimes \mathbf{n} \\
&= \frac{\partial\eta^1}{\partial\theta^1}\mathbf{g}_1(\eta^\alpha) \otimes \mathbf{g}^1(\theta^\alpha) + \frac{1-\kappa_1 Z}{1-\kappa_2 Z}\frac{\partial\eta^1}{\partial\theta^2}\mathbf{g}_1(\eta^\alpha) \otimes \mathbf{g}^2(\theta^\alpha) \\
&\quad + \frac{1-\kappa_2 Z}{1-\kappa_1 Z}\frac{\partial\eta^2}{\partial\theta^1}\mathbf{g}_2(\eta^\alpha) \otimes \mathbf{g}^1(\theta^\alpha) + \frac{\partial\eta^2}{\partial\theta^2}\mathbf{g}_2(\eta^\alpha) \otimes \mathbf{g}^2(\theta^\alpha) + \mathbf{n}(\eta^\alpha) \otimes \mathbf{n}(\theta^\alpha),
\end{aligned}
\tag{56}
$$

In Eq. (56), the covariant base $\{\mathbf{g}_1, \mathbf{g}_2, \mathbf{n}\}$ is evaluated at the position $\mathbf{s}(\eta^\alpha)$ on $\mathcal{S}_i$ and the contravariant base $\{\mathbf{g}^1, \mathbf{g}^2, \mathbf{n}\}$ is evaluated at the position $\mathbf{s}(\theta^\alpha)$ on $\mathcal{S}_r$. In the second step, we consider the deformation of the shell from the intermediate configuration $\mathcal{K}_i$ to the current configuration $\mathcal{K}_t$ (i.e., the shape change of the base surface from $\mathcal{S}_i$ to $\mathcal{S}_t$). As shown in Fig. 3, $\mathcal{S}_i$ and $\mathcal{S}_t$ possess the same parametric variable region Ω_r^* in the $\eta^1\eta^2$-plane. Besides

29

that, the coordinate curves of $\{\eta^\alpha\}$ constitute the net of curvature lines on these two surfaces. Thus, the formulas (42) and (44) obtained in section 3.1 should be applicable in this case. The growth tensor that can induce the shape change from $\mathcal{S}_i$ to $\mathcal{S}_t$ is then given by

$$
\begin{aligned}
\mathbb{G}_1 = {} & \left[1 + Z\left(\kappa_1^* - \frac{L}{E}\right)\right] \sqrt{\frac{E}{E^*}} \mathbf{g}_1(\eta^\alpha) \otimes \mathbf{g}^1(\eta^\alpha) \\
& + \left[1 + Z\left(\kappa_2^* - \frac{N}{G}\right)\right] \sqrt{\frac{G}{G^*}} \mathbf{g}_2(\eta^\alpha) \otimes \mathbf{g}^2(\eta^\alpha) + \mathbf{n}(\eta^\alpha) \otimes \mathbf{n}(\eta^\alpha).
\end{aligned}
\tag{57}
$$

In Eq. (57), $\{E, G, L, N\}$ are the fundamental quantities of surface $\mathcal{S}$ calculated with the parametric equation $\mathbf{x}^*(\eta^\alpha)$. $\{E^*, G^*\}$ and $\{\kappa_1^*, \kappa_2^*\}$ are the fundamental quantities and principal curvatures of surface $\mathcal{S}_i$ calculated with the parametric equation $\mathbf{s}(\eta^\alpha)$. It can be directly verified that

$$
\mathbb{G}_1 \mathbb{F}_0 = \mathbb{Q} \mathbb{G},
\tag{58}
$$

where $\mathbb{Q}$ is the rotation tensor

$$
\mathbb{Q} = \mathbf{g}_1(\eta^\alpha) \otimes \mathbf{g}^1(\theta^\alpha) + \mathbf{g}_2(\eta^\alpha) \otimes \mathbf{g}^2(\theta^\alpha) + \mathbf{n}(\eta^\alpha) \otimes \mathbf{n}(\theta^\alpha),
\tag{59}
$$

and

$$
\begin{aligned}
\mathbb{G} = {} & \left[1 + Z\left(\kappa_1^* - \frac{L}{E}\right)\right] \sqrt{\frac{E}{E^*}} \frac{\partial \eta^1}{\partial \theta^1} \mathbf{g}_1(\theta^\alpha) \otimes \mathbf{g}^1(\theta^\alpha) \\
& + \left[1 + Z\left(\kappa_1^* - \frac{L}{E}\right)\right] \sqrt{\frac{E}{E^*}} \left(\frac{1 - \kappa_1 Z}{1 - \kappa_2 Z}\right) \frac{\partial \eta^1}{\partial \theta^2} \mathbf{g}_1(\theta^\alpha) \otimes \mathbf{g}^2(\theta^\alpha) \\
& + \left[1 + Z\left(\kappa_2^* - \frac{N}{G}\right)\right] \sqrt{\frac{G}{G^*}} \left(\frac{1 - \kappa_2 Z}{1 - \kappa_1 Z}\right) \frac{\partial \eta^2}{\partial \theta^1} \mathbf{g}_2(\theta^\alpha) \otimes \mathbf{g}^1(\theta^\alpha) \\
& + \left[1 + Z\left(\kappa_2^* - \frac{N}{G}\right)\right] \sqrt{\frac{G}{G^*}} \frac{\partial \eta^2}{\partial \theta^2} \mathbf{g}_2(\theta^\alpha) \otimes \mathbf{g}^2(\theta^\alpha) + \mathbf{n}(\theta^\alpha) \otimes \mathbf{n}(\theta^\alpha).
\end{aligned}
\tag{60}
$$

Tensor $\mathbb{G}$ given in (60) is just the growth tensor that can result in the shape change of the base surface of the shell from $\mathcal{S}_r$ to $\mathcal{S}$ in the general case, which is consistent with the growth tensor obtained in (45) for the special case.

30

We provide some further analyses on the deformation gradient (or growth) tensors obtained in the two-step deformation process. In the first step, the deformation gradient tensor $\mathbb{F}_0$ corresponding to the shape change of the shell from $\mathcal{K}_r$ to $\mathcal{K}_i$ (i.e., the base surface changes from $\mathcal{S}_r$ to $\mathcal{S}_i$) is given in Eq. (56), which has a general form and is difficult to be realized in reality. However, as mentioned before, $\mathcal{S}_r$ and $\mathcal{S}_i$ can be viewed as the different subregions in a large surface (cf. Figs. 7c and 8c). In the second step, the growth tensor $\mathbb{G}_1$ corresponding to the shape change of the shell from $\mathcal{K}_i$ to $\mathcal{K}_t$ (i.e., the base surface changes from $\mathcal{S}_i$ to $\mathcal{S}_t$) is given in Eq. (57), which has a diagonal form and is easier to be realized. In practical conditions, to generate the target configuration $\mathcal{K}_t$ of the shell, one may first cut a shell sample with the base surface $\mathcal{S}_i$ from a large shell (cf. the surfaces $\mathcal{S}_i$ shown in Figs. 7c and 8c), and then generate the shape change of the shell sample from $\mathcal{S}_i$ to $\mathcal{S}_t$ according to the growth tensor $\mathbb{G}_1$ (e.g., arrange fibres along the curvature lines of surface $\mathcal{S}_i$).

3.3. A theoretical scheme for shape-programming

Based on the above preparations, we propose a theoretical scheme for shape-programming of a thin hyperelastic shell through differential growth. The flowchart of this scheme is shown in Fig. 4, which contains the following steps:

- With the given reference configuration $\mathcal{K}_r$ of the shell, we need to identify the parametric equation $\mathbf{s}(\theta^\alpha)$ for the initial shape of the base surface $\mathcal{S}_r$, which is defined on the region Ω_r of the $\theta^1\theta^2$-plane. By using $\mathbf{s}(\theta^\alpha)$, the fundamental quantities $\{E_r, G_r, L_r, N_r\}$ and the principal curvatures $\{\kappa_1, \kappa_2\}$ of surface $\mathcal{S}_r$ can be calculated.

31

```
┌─────────────────────────────────────────┐
│   Identify the reference configuration    │
│   of base surface 𝒮_r with the            │
│   parametric equation 𝒔(θ^α)              │
└─────────────────────────────────────────┘
                    │
                    ▼
┌─────────────────────────────────────────┐
│   Choose the target shape of the base     │
│   surface 𝒮 with the parametric           │
│   equation 𝒙^(0)(θ^α)                     │
└─────────────────────────────────────────┘
                    │
                    ▼
┌─────────────────────────────────────────┐
│   Calculate the fundamental quantities    │
│   {E, F, G} and {L, M, N} of 𝒮 by         │
│   using 𝒙^(0)(θ^α)                        │
└─────────────────────────────────────────┘
                    │
                    ▼
            Check F = 0 and M = 0 ?  ──── Yes ──┐
                    │                            │
                    │ No                         │
                    ▼                            │
┌─────────────────────────────────────────┐     │
│   Conduct variable change {θ^α} → {η^α}   │     │
│   and identify the new parametric         │     │
│   variable region Ω_r^*                   │     │
└─────────────────────────────────────────┘     │
                    │                            │
                    ▼                            │
┌─────────────────────────────────────────┐     │
│   Derive the parametric equation          │     │
│   𝒙^*(η^α) and generate orthogonal        │     │
│   curvature curves net on 𝒮              │     │
└─────────────────────────────────────────┘     │
                    │                            │
                    ▼                            │
┌─────────────────────────────────────────┐     │
│   Construct the intermediate shape of     │     │
│   the base surface 𝒮_i with the           │     │
│   parametric equation 𝒔(η^α)              │     │
└─────────────────────────────────────────┘     │
                    │                            │
                    ▼                            │
┌─────────────────────────────────────────┐     │
│   Calculate the growth tensor 𝔾           │◄────┘
│   according to the result given in        │
│   Eq. (60)                                │
└─────────────────────────────────────────┘
                    │
                    ▼
┌─────────────────────────────────────────┐
│   Verify the accuracy of the growth       │
│   tensor                                  │
└─────────────────────────────────────────┘
```
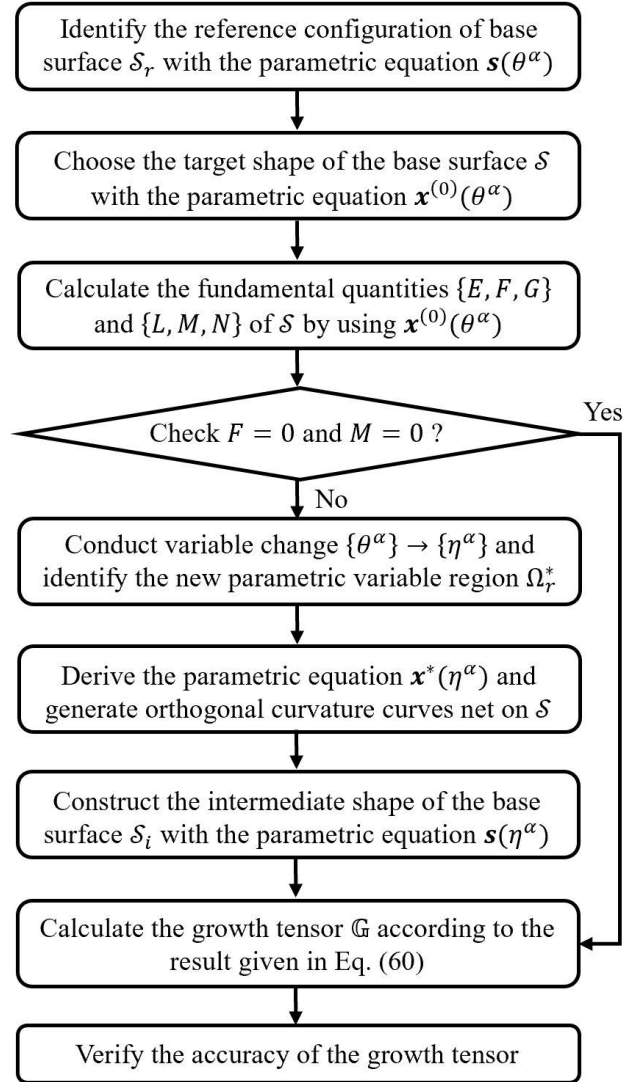
Figure 4: Flowchart of the theoretical scheme for shape-programming of a thin hyperelastic shell through differential growth.

- We choose the target shape of the base surface $\mathcal{S}$, which has the parametric equation $\mathbf{x}^{(0)}(\theta^\alpha)$ defined on Ω_r.

- The fundamental quantities $\{E, F, G\}$ and $\{L, M, N\}$ of surface $\mathcal{S}$ are calculated by using the parametric equation $\mathbf{x}^{(0)}(\theta^\alpha)$. In the case $F = 0$ and $M = 0$, it is known that the parametric curves net of $\{\theta^\alpha\}$ is already an orthogonal net of curvature lines (Chen, 2017). Then, the growth tensor $\mathbb{G}$ can be obtained from Eq. (45).

- If F and M are not both equal to zero, we need to conduct the variable change from $\{\theta^\alpha\}$ to $\{\eta^\alpha\}$, which yields a bijection from Ω_r to a new region Ω_r^* in the $\eta^1\eta^2$-plane. The explicit expressions of the variable change should be calculated from the differential forms given in (51), where the integrating factors A_1^* and A_2^* need to be determined in advance.

- After the variable change, the surface $\mathcal{S}$ has a new parametric equation $\mathbf{x}^*(\eta^\alpha)$ defined on Ω_r^*. The coordinate curves of $\{\eta^\alpha\}$ constitute an orthogonal net of curvature lines on $\mathcal{S}$.

- By virtue of the variable change, an intermediate shape of the base surface $\mathcal{S}_i$ can be constructed, which has the parametric equation $\mathbf{s}(\theta^\alpha)$ defined on Ω_r and the parametric equation $\mathbf{s}^*(\eta^\alpha)$ defined on Ω_r^*. The associated geometrical quantities of $\mathcal{S}_i$ are also calculated.

- Based on the above results, the growth tensor $\mathbb{G}$ is calculated from Eq. (60), which results in the shape change of the base surface of the shell from $\mathcal{S}_r$ to $\mathcal{S}$.

- Finally, to check the correctness and accuracy of this scheme, the obtained growth tensor (or growth functions) is incorporated in a finite element analysis (we use Abaqus), and the growth-induced deformation of the shell is simulated.

Remarks:

- In the above proposed theoretical scheme, we focus on the determination of the growth tensor that can induce the shape change of the shell from $\mathcal{S}_r$ to $\mathcal{S}$. In reality, there is another problem. That is, how to generate the growth field in the shell sample corresponding to the obtained growth tensor (some simple discussions on this issue have been given in subsections 3.1 and 3.2). For different mechanisms of growth of soft materials, one needs to find different ways to solve this problem.

- To verify the correctness of the obtained growth tensor, we will conduct numerical simulations (cf. the numerical simulation results in section 4). In the numerical simulations, the growth tensor will be used as the control quantity, which changes from the identity tensor $\mathbb{I}$ to the target tensor through some prescribed paths. It should be noted that corresponding to the same growth tensor, the shell sample may have different equilibrium state (i.e., the shell equation system have multiple solutions). Therefore, during the numerical calculations, one may meet the problem of instability of the growth-induced deformation of the shell (which is also a problem in manufacturing intelligent soft devices through differential growth). The problem of instability is an important issue that needs to be investigated systematically in the future work. To

overcome the problem of instability, one possible approach is to divide the whole growing process into several stages. During each stage, the target shape of the shell or the change of the growth tensor will be prescribed properly, such that the deformation of the shell is not very large. In this case, the possibility to trigger the instability phenomena of the shell sample will be reduced.

4. Examples

In this section, some typical examples will be studied to demonstrate the feasibility and efficiency of the analytical framework proposed in section 3 for shape-programming of thin hyperelastic shells through differential growth.

For the purpose of illustration, the reference configuration $\mathcal{K}_r$ of the shell is selected to be a cylindrical shell, which occupies the region $[R_0, R_0 + 2h] \times [0, \Theta_0] \times [0, l]$ within a cylindrical coordinate system in $\mathcal{R}^3$. The base surface $\mathcal{S}_r$ of the shell has the following parametric equation

$$\mathbf{s}(\theta^1, \theta^2) = \{R_0 \cos(\theta^1), R_0 \sin(\theta^1), \theta^2\}, \quad 0 \le \theta^1 \le \Theta_0, \ 0 \le \theta^2 \le l, \quad (61)$$

where θ^1 and θ^2 are the parametric variables. It is clear that the coordinate curves of θ^1 and θ^2 constitute a net of curvature lines on $\mathcal{S}_r$. Besides that, we denote $Z = R - R_0 \ (R_0 \le R \le R_0 + 2h)$ as the thickness variable of the shell. From the parametric equation (61), we obtain the following covariant and contravariant base vectors on $\mathcal{S}_r$

$$\mathbf{g}_1 = R_0 \left[-\sin(\theta^1)\mathbf{e}_1 + \cos(\theta^1)\mathbf{e}_2 \right], \quad \mathbf{g}^1 = \frac{\mathbf{g}_1}{R_0^2},$$

$$\mathbf{g}_2 = \mathbf{g}^2 = \mathbf{e}_3, \quad \mathbf{g}_3 = \mathbf{g}^3 = \mathbf{n} = \cos(\theta^1)\mathbf{e}_1 + \sin(\theta^1)\mathbf{e}_2. \quad (62)$$

35

The geometrical quantities of surface $\mathcal{S}_r$ are given by

$$E_r = R_0^2, \quad G_r = 1, \quad L_r = -R_0,$$
$$N_r = 0, \quad \kappa_1 = -1/R_0, \quad \kappa_2 = 0. \tag{63}$$

4.1. Examples without change of variables

First, the target shape of the base surface $\mathcal{S}$ is selected to be a surface of revolution, which has the following parametric equation

$$\mathbf{x}^{(0)}(\theta^1, \theta^2) = \{u(\theta^2)\cos(\theta^1), u(\theta^2)\sin(\theta^1), v(\theta^2)\}, \quad 0 \le \theta^1 \le \Theta_0, \ 0 \le \theta^2 \le l, \tag{64}$$

where $u(\theta^2)$ and $v(\theta^2)$ are arbitrarily smooth functions. Notice that both $\mathcal{S}_r$ and $\mathcal{S}$ have the parametric variable region $\Omega_r = [0, \Theta_0] \times [0, l]$. Corresponding to the parametric equation (64), the following first and second fundamental quantities of surface $\mathcal{S}$ are obtained

$$E = u^2, \quad F = 0, \quad G = u'^2 + v'^2,$$
$$L = -\frac{u^2 v'}{\sqrt{u^2\left(u'^2 + v'^2\right)}}, \quad M = 0, \quad N = \frac{u\left(v'u'' - u'v''\right)}{\sqrt{u^2\left(u'^2 + v'^2\right)}}. \tag{65}$$

Since $F = 0$ and $M = 0$, it is known that the θ^1- and θ^2-coordinate curves have already constituted an orthogonal net of curvature lines on $\mathcal{S}$. Therefore, the growth tensor in the shell should be set according to (45), which contains the growth functions

$$\lambda_1^{(0)} = |u|, \quad \lambda_2^{(0)} = \sqrt{u'^2 + v'^2},$$
$$\lambda_1^{(1)} = -\frac{|u|}{R_0} + \frac{v'}{\sqrt{u'^2 + v'^2}}, \quad \lambda_2^{(1)} = \frac{u\left(u'v'' - v'u''\right)}{|u|\left(u'^2 + v'^2\right)}. \tag{66}$$

For concreteness, we consider four kinds of revolution surfaces inspired by biological tissues, i.e., the sweet melon, the morning glory, the trachea and

36

the apple. The parametric equations and the corresponding growth functions of these surfaces are listed in (67)-(70).

- Sweet melon $(0 \leq \theta^1 \leq \pi, \quad 0 \leq \theta^2 \leq 4)$:

$$
\begin{cases}
x^{(0)} = 4\cos(2\theta^1)\cos\left(\dfrac{9}{40}\pi(\theta^2 - 2)\right), \\[2mm]
y^{(0)} = 4\sin(2\theta^1)\cos\left(\dfrac{9}{40}\pi(\theta^2 - 2)\right), \\[2mm]
z^{(0)} = -4\cos\left(\dfrac{1}{40}\pi(9\theta^2 + 2)\right), \\[2mm]
\lambda_1 = 8\cos\left(\dfrac{9}{40}\pi(\theta^2 - 2)\right), \quad \lambda_2 = \dfrac{9}{40}\pi(Z + 4).
\end{cases}
\tag{67}
$$

- Morning glory $(0 \leq \theta^1 \leq \pi, \quad 0 \leq \theta^2 \leq 4)$

$$
\begin{cases}
x^{(0)} = -(1 + \theta^2)\cos(2\theta^1), \\[2mm]
y^{(0)} = -(1 + \theta^2)\sin(2\theta^1), \\[2mm]
z^{(0)} = 6 - \dfrac{1}{8}\left(7 - 2\theta^2\right)^2, \\[2mm]
\lambda_1 = \dfrac{1}{2}(\theta^2 + 1)\left[4 - \dfrac{4(2\theta^2 - 7)Z}{(\theta^2 + 1)\sqrt{4\theta^2\,(\theta^2 - 7) + 53}} - Z\right], \\[2mm]
\lambda_2 = \sqrt{\theta^2(\theta^2 - 7) + \dfrac{53}{4} - \dfrac{4Z}{4\theta^2\,(\theta^2 - 7) + 53}}.
\end{cases}
\tag{68}
$$

- Trachea $(0 \leq \theta^1 \leq 2\pi, \quad 0 \leq \theta^2 \leq 4)$

$$\begin{cases} x^{(0)} = \dfrac{1}{5}\cos\theta^1 \left[20 + \sin(2\pi\theta^2)\right], \\[2mm] y^{(0)} = \dfrac{1}{5}\sin\theta^1 \left[20 + \sin(2\pi\theta^2)\right], \\[2mm] z^{(0)} = 2(2 + \theta^2), \\[2mm] \lambda_1 = -\dfrac{1}{20}(Z - 4)\sin(2\pi\theta^2) + 4 + Z\left(\dfrac{5\sqrt{2}}{\sqrt{\pi^2\cos(4\pi\theta^2) + \pi^2 + 50}} - 1\right), \\[4mm] \lambda_2 = \dfrac{1}{5}\sqrt{2}\sqrt{\pi^2\cos(4\pi\theta^2) + \pi^2 + 50} + \dfrac{20\pi^2 Z\sin(2\pi\theta^2)}{\pi^2\cos(4\pi\theta^2) + \pi^2 + 50}. \end{cases}$$

$$(69)$$

- Apple $(0 \le \theta^1 \le 2\pi, \quad 0 \le \theta^2 \le 4)$

$$\begin{cases} x^{(0)} = 8\cos\theta^1\cos^2\left(\dfrac{\pi\theta^2}{4}\right), \\[3mm] y^{(0)} = 8\sin\theta^1\cos^2\left(\dfrac{\pi\theta^2}{4}\right), \\[3mm] z^{(0)} = -6\sin\left(\dfrac{\pi\theta^2}{2}\right), \\[3mm] \lambda_1 = \dfrac{-3\sqrt{2}Z\cos\left(\frac{\pi\theta^2}{2}\right)}{\sqrt{5\cos(\pi\theta^2) + 13}} - 2(Z - 4)\cos^2\left(\dfrac{\pi\theta^2}{4}\right), \\[4mm] \lambda_2 = \pi\left[\dfrac{\sqrt{5\cos(\pi\theta^2) + 13}}{\sqrt{2}} - \dfrac{6Z}{5\cos(\pi\theta^2) + 13}\right]. \end{cases}$$

$$(70)$$

To verify the accuracy of the obtained growth functions, we also conduct numerical simulations by using the UMAT subroutine in ABAQUS, where the constitutive relation of a compressible neo-Hookean material is adopted. The Poisson's ratio of the material is chosen to $\nu = 0.4995$ to capture the effect of elastic incompressibility. The initial cylindrical shell has the dimensions $R_0 = 4$, $h = 0.01$ and $l = 4$. The value of Θ_0 is set to be π or 2π depending upon the cases, which corresponds to a semi-cylindrical shell or a whole cylindrical shell, respectively. The shell sample is meshed into 15800 elements when

$\Theta_0 = \pi$ and 20160 elements when $\Theta_0 = 2\pi$. The element type is selected to be C3D8IH (8-node linear brick, hybrid, linear pressure, incompatible modes). As the surfaces of the shell sample are supposed to be traction-free, there is no further manipulations needs to be conducted. Only except that the displacement components of three selected points are restricted to eliminate the possibility of rigid body motion (cf. Fig. 5). In the numerical simulations with ABAQUS, the model type is standard and the analysis type is static, general. The growth functions $\lambda_1 = \lambda_1^{(0)} + Z\lambda_1^{(1)}$ and $\lambda_2 = \lambda_2^{(0)} + Z\lambda_2^{(1)}$ are incorporated as the state variables in the UMAT subroutine, which change gradually from 1 to the target values as those given in (67)-(70) during the time regime $t \in [0, 1]$. The time increment size of the load steps is set to be automatic change between 10^{-6} to 0.5. By properly choosing the evolution paths of the growth functions (cf. Appendix B for some further discussions), the growth-induced deformations of the shell sample can be simulated. For convenience of the readers, the UMAT files and the ABAQUS input files for the examples studied in this subsection are provided in the supplementary materials.

In Fig. 6, we show the numerical simulation results. It can be seen that the grown states of the shells are in good agreement with the target shapes. Thus, the correctness of the obtained growth functions can be verified. It should be pointed out that here we only try to mimic the outer surface shapes of the different biological tissues, but do not aim to reveal the underlying mechanisms responsible for the growth of the biological tissues. In fact, the shape changes of some biological tissues (e.g., apple, sweet melon) during the growing processes should be attributed to the inherently volumetric growth.

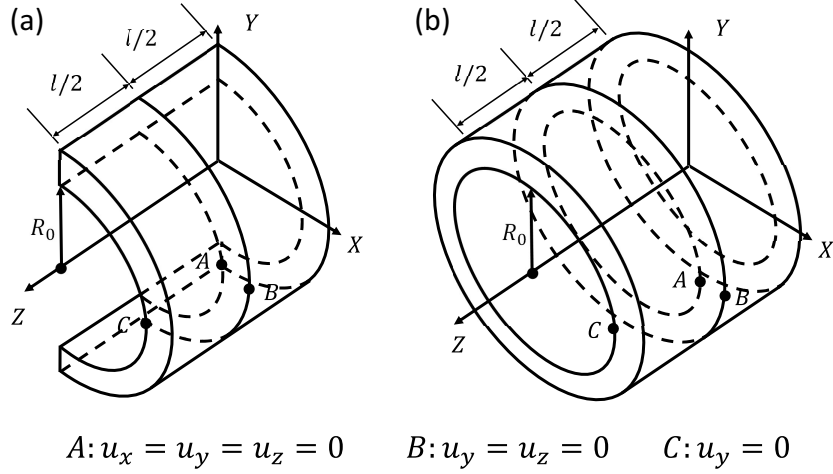$$A: u_x = u_y = u_z = 0 \qquad B: u_y = u_z = 0 \qquad C: u_y = 0$$

Figure 5: Illustration of removing the rigid body motion by restricting the displacement components of three selected points: (a) the semi cylindrical shell; (b) the whole cylindrical shell.

4.2. Examples with change of variables

To further demonstrate the efficiency of the proposed theoretical scheme, we study two more examples, in which the target shapes are chosen to be the Cereus Forbesii Spiralis and the tendril of pumpkin.

For the case of Cereus Forbesii Spiralis, the parametric equation of the target surface $\mathcal{S}$ is

$$\mathbf{x}^{(0)}(\theta^1, \theta^2) = \left\{ \frac{2\theta^1}{\pi} \sin(\pi\theta^2), \frac{2\theta^1}{\pi} \cos(\pi\theta^2), \theta^2 \right\}, \tag{71}$$

where the region of the parametric variable is chosen to be $\Omega_r = [0, \pi] \times [0, 4]$. Corresponding to this parametric equation, one can obtain the first and second fundamental quantities as follows

$$
\begin{aligned}
E = 4/\pi^2, \quad F = 0, \quad G = 1 + 4{\theta^1}^2, \\
L = 0, \quad M = 2/\sqrt{1 + 4{\theta^1}^2}, \quad N = 0.
\end{aligned}
\tag{72}
$$

40
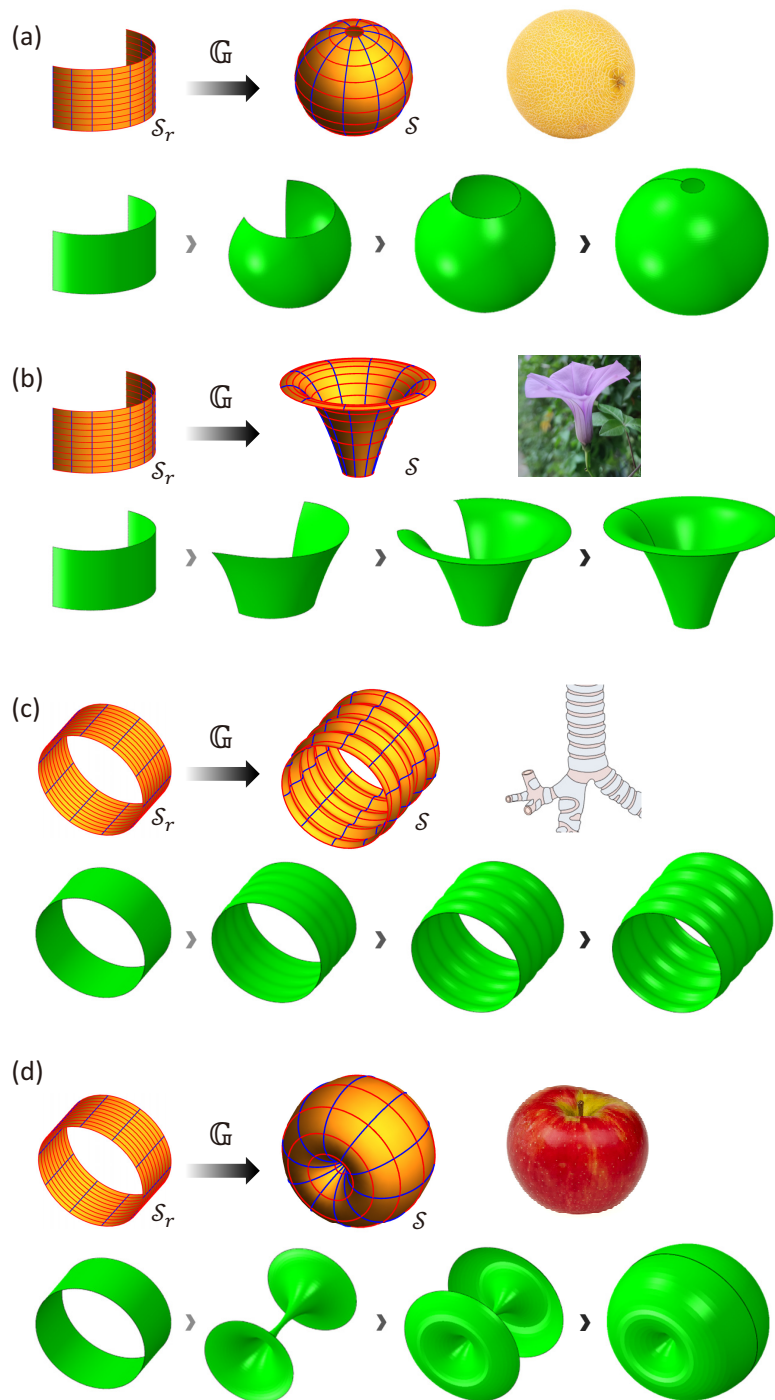
Figure 6: Numerical simulation results on the growing processes of the shells with the target surfaces and growth functions listed in (67)-(70): (a) the sweet melon; (b) the morning glory; (c) the trachea; (d) the apple.
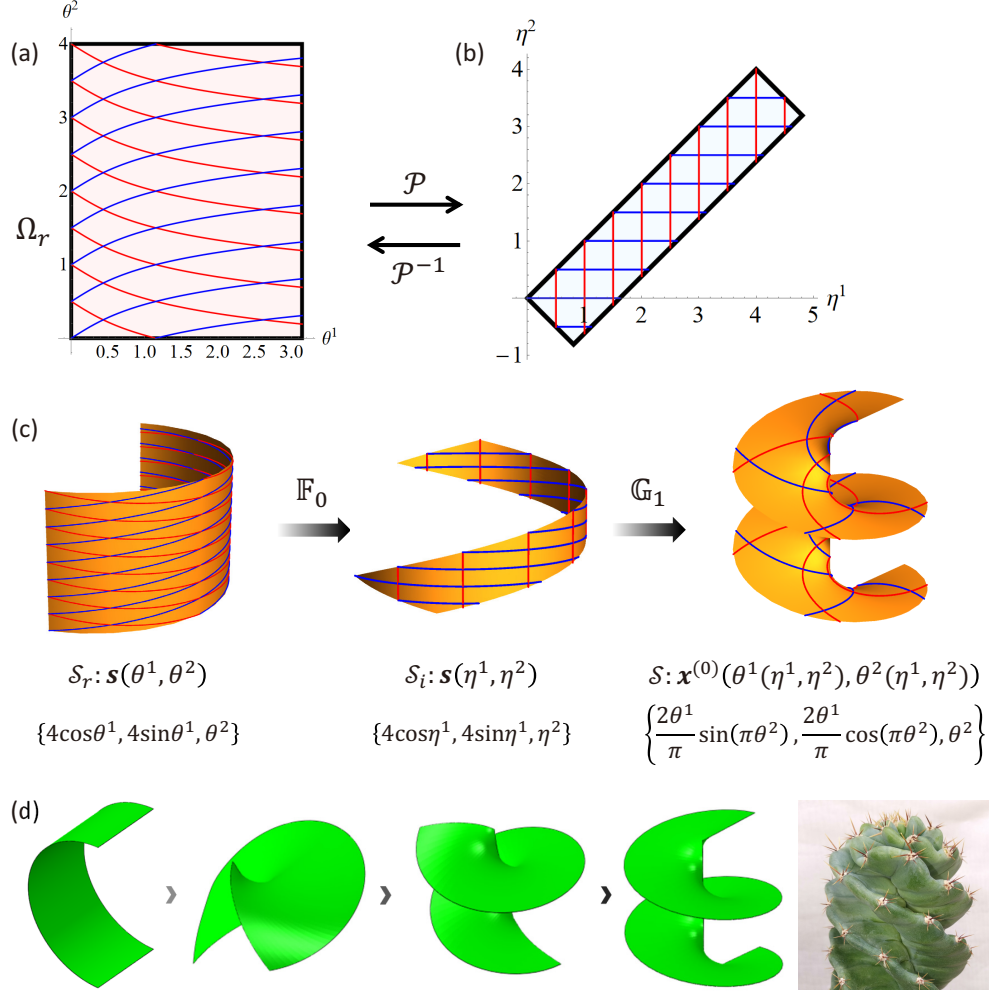
41

Figure 7: Change of variables between $\{\theta^1, \theta^2\}$ and $\{\eta^1, \eta^2\}$, and the decomposition of the growth process for generating Cereus Forbesii Spiralis: (a) the original region Ω_r on the parametric plane $\theta^1\theta^2$; (b) the new region Ω_r^* on the parametric plane $\eta^1\eta^2$; (c) the base surface $\mathcal{S}_r$ in the referential configuration $\mathcal{K}_r$, the base surface $\mathcal{S}_i$ in the intermediate configuration $\mathcal{K}_i$, and the target base surface $\mathcal{S}$ in the current configuration $\mathcal{K}_t$; (d) the simulated growing process for generating the Cereus Forbesii Spiralis configuration of the shell.

42

As the quantity $M \neq 0$, we need to conduct the change of variables from (θ^1, θ^2) to (η^1, η^2). According to the procedure of variable change introduced in section 3.2, we have

$$\eta^1\left(\theta^1, \theta^2\right) = \frac{\text{arcsinh}(2\theta^1)}{\pi} + \theta^2, \quad \eta^2\left(\theta^1, \theta^2\right) = -\frac{\text{arcsinh}(2\theta^1)}{\pi} + \theta^2. \quad (73)$$

After the variable transformation, the original region Ω_r in the $\theta^1\theta^2$- plane is mapped into a new region Ω_r^* in the $\eta^1\eta^2$-plane, which is shown in Fig. 7(b). On the region Ω_r^*, a new surface $\mathcal{S}_i$ is defined as follows

$$\mathcal{S}_i : \mathbf{s}^* = \{R_0 \cos \eta^1, R_0 \sin \eta^1, \eta^2\}, \quad \eta^\alpha \in \Omega_r^*. \quad (74)$$

Notice that the cylindrical shell $\mathcal{S}_r$ defined by (61) and the surface $\mathcal{S}_i$ defined by (74) have the same parametric equation, but their parametric variable regions are different. As shown in Fig. 7c, both $\mathcal{S}_r$ and $\mathcal{S}_i$ can be viewed as a subregion cutting from a large cylindrical surface with radius $R_0 = 4$. Also, the coordinate curves of $\{\eta^\alpha\}$ (i.e., the black and red curves in Fig. 7) constitute the orthogonal nets of curvature lines on both $\mathcal{S}_i$ and $\mathcal{S}$. By choosing $\mathcal{S}_i$ as the base surface, we define an intermediate configuration $\mathcal{K}_i$ according to (55), then the whole growth process can be divided into two steps: $\mathcal{K}_r \to \mathcal{K}_i$ and $\mathcal{K}_i \to \mathcal{K}_t$. For the first step, according to (56) the deformation gradient $\mathbb{F}_0$ is given by

$$\mathbb{F}_0 = \frac{2}{\pi\sqrt{1 + 4\theta^{1^2}}} \mathbf{g}_1(\eta^\alpha) \otimes \mathbf{g}^1(\theta^\alpha) + (1 + Z/R_0)\mathbf{g}_1(\eta^\alpha) \otimes \mathbf{g}^2(\theta^\alpha)$$

$$- \frac{2}{\pi\left(Z/R_0 + 1\right)\sqrt{1 + 4\theta^{1^2}}} \mathbf{g}_2(\eta^\alpha) \otimes \mathbf{g}^1(\theta^\alpha) + \mathbf{g}_2(\eta^\alpha) \otimes \mathbf{g}^2(\theta^\alpha) \quad (75)$$

$$+ \mathbf{n}(\eta^\alpha) \otimes \mathbf{n}(\theta^\alpha).$$

For the second step, the following growth tensor $\mathbb{G}_1$ on domain (η^1, η^2) is

43

obtained according to (57)

$$
\begin{aligned}
\mathbb{G}_1 =& \mathbf{g}_1(\eta^\alpha) \otimes \mathbf{g}^1(\eta^\alpha) \left[\frac{1}{8} \sqrt{\cosh(\pi(\eta^1 - \eta^2)) + 1} \right. \\
& \left. - \frac{Z\left(16\pi\sqrt{\cosh^4\left(\frac{1}{2}\pi(\eta^1 - \eta^2)\right)} + \cosh^2(\pi(\eta^1 - \eta^2)) + 2\cosh(\pi(\eta^1 - \eta^2)) + 1\right)}{32(\cosh(\pi(\eta^1 - \eta^2)) + 1)^{3/2}} \right] \\
& + \mathbf{g}_2(\eta^\alpha) \otimes \mathbf{g}^2(\eta^\alpha) \left[\frac{1}{2}\sqrt{\cosh(\pi(\eta^1 - \eta^2)) + 1} + \frac{2\pi Z\sqrt{\cosh^4\left(\frac{1}{2}\pi(\eta^1 - \eta^2)\right)}}{(\cosh(\pi(\eta^1 - \eta^2)) + 1)^{3/2}} \right] \\
& + \mathbf{n}(\eta^\alpha) \otimes \mathbf{n}(\eta^\alpha).
\end{aligned}
\tag{76}
$$

Then the tensor $\mathbb{G}$ generating the shape change from $\mathcal{S}_r$ to $\mathcal{S}$ can be calculated from (60). To verify the correctness of these growth functions, we also simulate the growth process of Cereus Forbesii Spiralis in ABAQUS. The setting of the numerical simulations is same as that introduced in the section 4.1. The numerical results of this example are shown in Fig. 7d. It can be found that the final shape of the shell can fit the target shape quite well.

For the case of pumpkin tendril, the parametric equation of the target surface $\mathcal{S}$ is

$$
\mathbf{x}^{(0)}(\theta^1, \theta^2) = \left\{ (\cos\theta^1 + 2)\cos\left(\frac{\pi\theta^2}{2}\right), (\cos\theta^1 + 2)\sin\left(\frac{\pi\theta^2}{2}\right), \sin\theta^1 + \theta^2 \right\},
\tag{77}
$$

where the region on the parametric plane is chosen to be $\Omega_r = [0, 2\pi] \times [0, 8]$. Corresponding to this parametric equation, one can obtain the first

44

and second fundamental quantities as follow

$$
\begin{aligned}
E &= 1, \quad F = \cos\theta^1, \quad G = \frac{1}{8}\left(\pi^2(8\cos(\theta^1) + \cos(2\theta^1)) + 9\pi^2 + 8\right), \\
L &= \frac{\sqrt{2}\pi(\cos(\theta^1) + 2)}{\sqrt{8\pi^2\cos(\theta^1) + (\pi^2 - 4)\cos(2\theta^1) + 9\pi^2 + 4}}, \\
M &= -\frac{\sqrt{2}\pi\sin^2(\theta^1)}{\sqrt{8\pi^2\cos(\theta^1) + (\pi^2 - 4)\cos(2\theta^1) + 9\pi^2 + 4}}, \\
N &= \frac{\pi^3\cos(\theta^1)(\cos(\theta^1) + 2)^2}{2\sqrt{2}\sqrt{8\pi^2\cos(\theta^1) + (\pi^2 - 4)\cos(2\theta^1) + 9\pi^2 + 4}}.
\end{aligned}
\tag{78}
$$

Note that the quantities $F \neq 0$ and $M \neq 0$, thus the change of variables from (θ^1, θ^2) to (η^1, η^2) is required. As shown in Fig.8(b), the original region Ω_r is mapped into a new region Ω_r^* through the change of variables. Following the same parametric equation, these two regions define surfaces $\mathcal{S}_r$ and $\mathcal{S}_i$ respectively, where $\mathcal{S}_r$ is a cylinder with radius $R_0 = 4$ and length $l = 8$, while $\mathcal{S}_i$ is an irregular shaped subregion cut from a cylinder with radius $R_0 = 4$ as follow

$$
\mathcal{S}_i : \mathbf{s}^* = \{R_0\cos\eta^1, R_0\sin\eta^1, \eta^2\}, \quad \eta^\alpha \in \Omega_r^*.
\tag{79}
$$

Also, the coordinate curves $\{\eta^\alpha\}$ (i.e., the black and red curves in Fig. 8) constitute an orthogonal curvature net on both $\mathcal{S}_i$ and $\mathcal{S}$. By choosing $\mathcal{S}_i$ as the base surface, we define an intermediate configuration $\mathcal{K}_i$. The whole shape morphing process can be divided into two steps: from $\mathcal{K}_r$ to $\mathcal{K}_i$ described by $\mathbb{F}_0$, and from $\mathcal{K}_i$ to $\mathcal{K}_t$ induced by $\mathbb{G}_1$. However, the analytical explicit expressions for integrating factors and (η^1, η^2) are difficult to obtain. Therefore the tensor $\mathbb{F}_0$ and $\mathbb{G}_1$ are calculated numerically in this case, and then the growth values are passed to the relating integration points of the elements in ABAQUS. According to the numerical results of this case shown

in Fig.8(d), it is known that the final shape of the shell can also fit the target shape quite well. The UMAT files and the ABAQUS input files for the two examples studied in this subsection are also provided in the supplementary materials.

5. Conclusions

In this paper, the problem of shape-programming of thin hyperelastic shells through differential growth was studied. First, a consistent finite-strain shell theory for modeling the growth-induced deformations of incompressible hyperelastic shells was introduced. Then, the problem of shape-programming was solved analytically under the stress-free condition, from which the explicit expressions of the growth functions in terms of the geometrical quantities (i.e., the first and second fundamental forms) of the target surfaces were derived. Based on these analytical results, a general theoretical scheme for shape-programming of thin hyperelastic shells through differential growth was proposed. To verify the correctness and efficiency of the theoretical scheme, some typical examples were studied, where the shape changes of soft material samples were simulated with the obtained growth functions. It was found that the simulated configurations of the soft material samples can fit the target surfaces quite well.

Since the formulas derived in the current work have relatively simple forms and are valid for general incompressible hyperelastic material, the presented theoretical scheme for shape-programming would have wide potential applications for design and manufacturing of intelligent soft devices. Furthermore, the analytical results can also shed light on understanding the mechanical be-
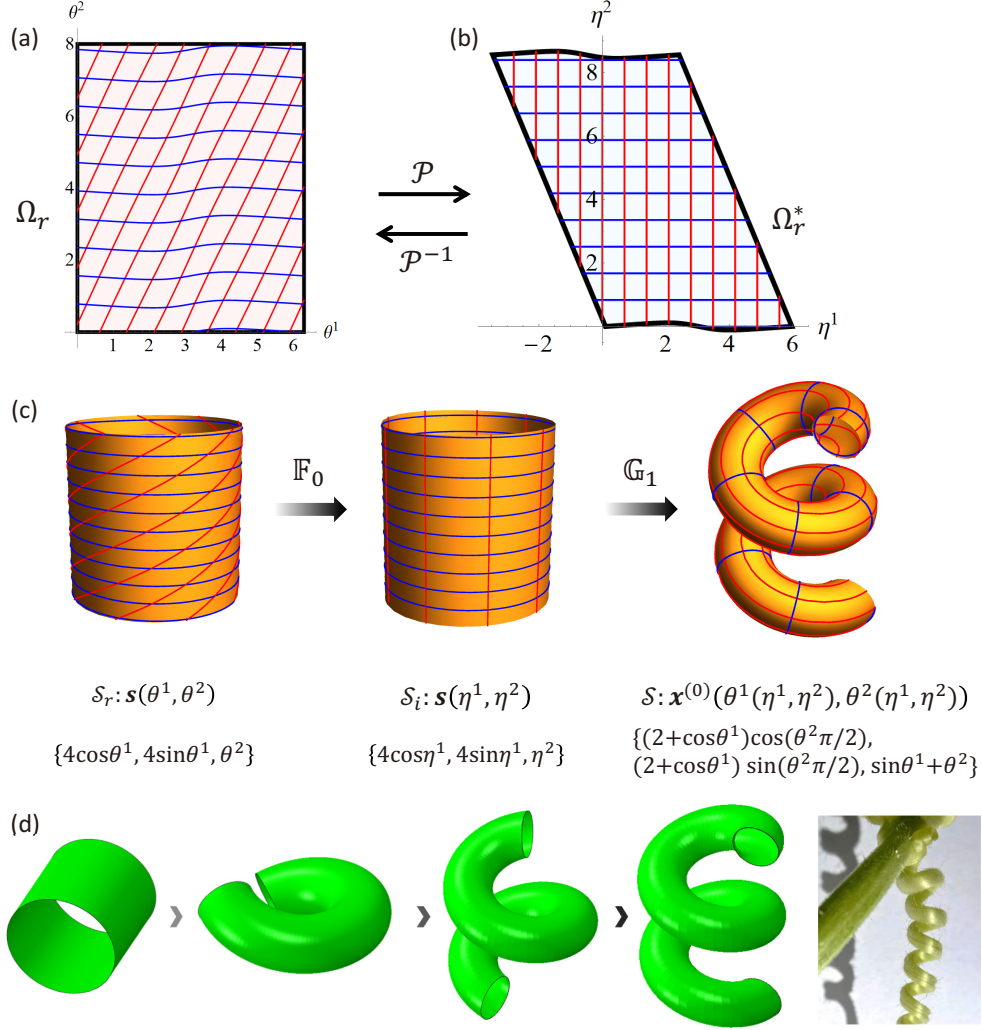
Figure 8: Change of variables between $\{\theta^1, \theta^2\}$ and $\{\eta^1, \eta^2\}$, and the decomposition of the growth process for generating tendril of pumpkin: (a) the original region Ω_r in the parametric plane $\theta^1\theta^2$; (b) the new region Ω_r^* in the parametric plane $\eta^1\eta^2$; (c) the base surface $\mathcal{S}_r$ in the referential configuration $\mathcal{K}_r$, the base surface $\mathcal{S}_i$ on the intermediate configuration $\mathcal{K}_i$, and the target base surface $\mathcal{S}$ in the current configuration $\mathcal{K}_t$; (d) the simulated growing process for generating the tendril of pumpkin configuration of the shell.

47

haviors of some soft biological tissues in nature during the growth processes. It should be pointed out that the current work still has some shortcomings that need to be tackled in future. One shortcoming is that the explicit expressions of growth tensor is derived based on the stress-free assumption. Therefore, they are not valid for shell samples subject to external loads or boundary restrictions. Additionally, the theoretical scheme is not applicable to complex 3D surfaces without explicit parametric equations. In that case, an efficient numerical scheme for shape-programming of complicated surfaces needs to be proposed. Besides that, the current work focus on the determination of the growth tensor corresponding to the target surface of the shell sample. In reality, one also needs to consider how to generate the growth field in the shell sample and how to tackle the problem of instability during the numerical simulation or manufacturing processes.

Supplementary documents

Movie 1: Growth processes of the shape-programming examples. The video of the growing processes of the six illustrative examples shown in Figs. 6, 7 and 8 is available at `https://github.com/Jeff97/growth-deformation-of-shell`.

ABAQUS input files and UMAT files: the ABAQUS input files for the shape-programming examples and the related UMAT files are also available at `https://github.com/Jeff97/growth-deformation-of-shell`.

Declaration of competing interest

The authors declare that they have no known competing financial interests or personal relationships that could have appeared to influence the work

reported in this paper.

Acknowledgments

Appendix A. Some results for incompressible neo-Hookean material

To obtain some concrete results on the unknowns ($\mathbf{x}^{(n)}$ and $p^{(n)}$), we further assume that the shell is made of neo-Hookean material with the following elastic strain-energy function

$$\phi(\mathbb{F}, \mathbb{G}) = J_G \phi_0(\mathbb{A}) = J_G C_0 \left[\mathrm{tr}(\mathbb{A}\mathbb{A}^T) - 3 \right], \tag{A.1}$$

where C_0 is a material constant. From the elastic strain-energy function $\phi(\mathbb{F}, \mathbb{G})$, the nominal stress tensor $\mathbb{S}$ is given by

$$\mathbb{S} = J_G \mathbb{G}^{-1} \left(2C_0 \mathbb{A}^T - p(R, Z)\mathbb{A}^{-1} \right). \tag{A.2}$$

For simplicity, we assume the shell is under traction-free condition. By taking series expansion on $Z = 0$ and through some truncation manipulation, a closed linear system for $\{\mathbf{x}^{(1)}, \mathbf{x}^{(2)}, p^{(0)}, p^{(1)}\}$ is formulated by (23) and $(24)_1$, combining with the boundary conditions $(25)_1$. Then the following expressions of $\{\mathbf{x}^{(1)}, \mathbf{x}^{(2)}, p^{(0)}, p^{(1)}\}$ in terms of $\mathbf{x}^{(0)}$ are solved

$$\mathbf{x}^{(1)} = \Lambda \frac{\mathbf{x}_N}{\Delta}, \quad p^{(0)} = 2C_0 \frac{\Lambda^2}{\Delta}, \tag{A.3}$$

49

$$\mathbf{x}^{(2)} = \frac{1}{\Delta^{5/2}} \mathbf{x}_N \left(\Lambda^2 t_9 + \frac{\Delta^2}{\Lambda^2} t_8 - \Delta^{3/2} t_1 \right) - \frac{1}{\Lambda^2} \mathbf{a}$$

$$+ \frac{1}{\Delta^3 \Lambda^3} \left[\mathbf{x}_{,1}^{(0)} \left(\Lambda^4 t_5 - \Delta^3 \lambda_2^{(0)} t_7 \right) + \mathbf{x}_{,2}^{(0)} \left(\Lambda^4 t_4 - \Delta^3 \lambda_1^{(0)} t_6 \right) \right], \quad \text{(A.4)}$$

$$p^{(1)} = 2C_0 \left(\frac{1}{\Lambda\sqrt{\Delta}} t_8 - \frac{2\Lambda}{\Delta} t_1 + \frac{\Lambda^3}{\Delta^{5/2}} t_9 \right),$$

where

$$\Lambda = \lambda_1^{(0)} \lambda_2^{(0)}, \quad \mathbf{x}_N = \mathbf{x}_{,1}^{(0)} \times \mathbf{x}_{,2}^{(0)}, \quad \Delta = \mathbf{x}_N \cdot \mathbf{x}_N,$$

$$B_{\alpha\beta} = \mathbf{g}_\alpha \cdot \mathbf{g}_{\beta,\alpha}, \quad \mathbf{a} = \left(\lambda_1^{(0)^2} \mathbf{x}_{,2,2}^{(0)} + \lambda_2^{(0)^2} \mathbf{x}_{,1,1}^{(0)} \right),$$

$$t_1 = (\kappa_1 + \kappa_2) \Lambda - \lambda_1^{(1)} \lambda_2^{(0)} - \lambda_1^{(0)} \lambda_2^{(1)},$$

$$t_2 = (B_{11} + B_{21}) \Lambda, \quad t_3 = (B_{12} + B_{22}) \Lambda,$$

$$t_4 = \Lambda (\Delta_{,1} F - \Delta_{,2} E) + \Delta [E (2\Lambda_{,2} + t_3) - F (2\Lambda_{,1} + t_2)],$$

$$t_5 = \Lambda (\Delta_{,2} F - \Delta_{,1} G) + \Delta [G (2\Lambda_{,1} + t_2) - F (2\Lambda_{,2} + t_3)],$$

$$t_6 = \lambda_{1,2}^{(0)} \Lambda + \lambda_1^{(0)} \left(t_3 - \lambda_{2,2}^{(0)} \lambda_1^{(0)} \right), \quad t_7 = \lambda_{2,1}^{(0)} \Lambda + \lambda_2^{(0)} \left(t_2 - \lambda_{1,1}^{(0)} \lambda_2^{(0)} \right),$$

$$t_8 = \left(\lambda_1^{(0)^2} N + \lambda_2^{(0)^2} L \right), \quad t_9 = (EN - 2FM + GL).$$

The expressions of $\mathbb{S}^{(0)}$ in terms of $\mathbf{x}^{(0)}$ are obtained by substituting $\mathbf{x}^{(1)}$ and $p^{(0)}$ into $(22)_1$

$$\mathbb{S}^{(0)} = 2C_0 \mathbf{g}_1 \otimes \left[\frac{\Lambda^3}{\Delta^2} (F \mathbf{x}_{,2}^{(0)} - G \mathbf{x}_{,1}^{(0)}) + \frac{\lambda_2^{(0)}}{\lambda_1^{(0)}} \mathbf{x}_{,1}^{(0)} \right]$$

$$+ 2C_0 \mathbf{g}_2 \otimes \left[-\frac{\Lambda^3}{\Delta^2} (F \mathbf{x}_{,1}^{(0)} - E \mathbf{x}_{,2}^{(0)}) + \frac{\lambda_1^{(0)}}{\lambda_2^{(0)}} \mathbf{x}_{,2}^{(0)} \right]. \quad \text{(A.5)}$$

Accordingly, expression of $\mathbb{S}^{(1)}$ is also obtained, where $\mathbf{x}^{(2)}$ and $p^{(1)}$ are kept

for brevity

$$
\begin{aligned}
\mathbb{S}^{(1)} =&\, 2C_0\mathbf{g}_1 \otimes \left[\frac{\left(-\lambda_1^{(1)}\lambda_2^{(0)} + \lambda_1^{(0)}\lambda_2^{(1)} + \Lambda\kappa_1\right)}{\lambda_1^{(0)2}}\mathbf{x}_{,1}^{(0)} - \frac{\Lambda^2}{\Delta}\mathbf{x}_{,2}^{(0)} \times \mathbf{x}^{(2)} \right.\\
&+ \frac{\Lambda^4}{\Delta^{5/2}}\left(N\mathbf{x}_{,1}^{(0)} - M\mathbf{x}_{,2}^{(0)}\right) + \frac{\lambda_2^{(0)}\left(\Delta\Lambda_{,1} - \Lambda\Delta_{,1}\right)}{\Delta^2\lambda_1^{(0)}}\mathbf{x}_N\\
&- \left. \frac{\Lambda\left(\kappa_2\Lambda^2 + p^{(1)}\Delta/(2C_0)\right)}{\Delta^2}\left(G\mathbf{x}_{,1}^{(0)} - F\mathbf{x}_{,2}^{(0)}\right) + \frac{\lambda_2^{(0)2}}{\Delta}\mathbf{x}_{N,1} \right]\\
&+ 2C_0\mathbf{g}_2 \otimes \left[\frac{\left(\lambda_1^{(1)}\lambda_2^{(0)} - \lambda_1^{(0)}\lambda_2^{(1)} + \Lambda\kappa_2\right)}{\lambda_2^{(0)2}}\mathbf{x}_{,2}^{(0)} + \frac{\Lambda^2}{\Delta}\mathbf{x}_{,1}^{(0)} \times \mathbf{x}^{(2)} \right.\\
&- \frac{\Lambda^4}{Q^{5/2}}\left(M\mathbf{x}_{,1}^{(0)} - L\mathbf{x}_{,2}^{(0)}\right) + \frac{\lambda_1^{(0)}\left(\Delta\Lambda_{,2} - \Lambda\Delta_{,2}\right)}{\Delta^2\lambda_2^{(0)}}\mathbf{x}_N\\
&+ \left. \frac{\Lambda\left(\kappa_1\Lambda^2 + p^{(1)}\Delta/(2C_0)\right)}{\Delta^2}\left(F\mathbf{x}_{,1}^{(0)} - E\mathbf{x}_{,2}^{(0)}\right) + \frac{\lambda_1^{(0)2}}{\Delta}\mathbf{x}_{N,2} \right]\\
&+ 2C_0\mathbf{n} \otimes \left[\left(-\frac{\Lambda t_1}{\Delta} - p^{(1)}/(2C_0)\right)\mathbf{x}_N + \Lambda\mathbf{x}^{(2)} \right.\\
&+ \frac{\Lambda^2}{\Delta^3}\left[\left(\Delta\Lambda_{,1} - \Lambda\Delta_{,1}\right)\left(G\mathbf{x}_{,1}^{(0)} - F\mathbf{x}_{,2}^{(0)}\right) - \left(\Delta\Lambda_{,2} - \Lambda\Delta_{,2}\right)\left(F\mathbf{x}_{,1}^{(0)} - E\mathbf{x}_{,2}^{(0)}\right)\right]\\
&+ \left. \frac{\Lambda^3}{\Delta^2}\left(\mathbf{x}_{N,2} \times \mathbf{x}_{,1}^{(0)} - \mathbf{x}_{N,1} \times \mathbf{x}_{,2}^{(0)}\right) \right].
\end{aligned}
$$

(A.6)

Note that $\mathbb{S}^{(1)}$ is also in terms of $\mathbf{x}^{(0)}$ with the use of (A.4).

In order to fulfil the goal of shape-programming, the growth functions $\lambda_1^{(0)}$, $\lambda_1^{(1)}$, $\lambda_2^{(0)}$ and $\lambda_2^{(1)}$ of an arbitrary target shape $\mathbf{x}^{(0)}$ need to be determined from shell equation system. Generally, the growth functions of a certain target shape may not be unique. To facilitate derivation, we assume all the components $\mathbb{S}^{(0)}$ and $\mathbb{S}^{(1)}$ in current configuration $\mathcal{K}_t$ are zero. It is clear that, under the stress-free assumption, the shell equation (28) and the boundary

conditions (29) are satisfied automatically.

First, all components of $\mathbb{S}^{(0)}$ in (A.5) are set to be zero

$$
\begin{cases}
\dfrac{\Lambda^3}{\Delta^2}(F\mathbf{x}_{,2}^{(0)} - G\mathbf{x}_{,1}^{(0)}) + \dfrac{\lambda_2^{(0)}}{\lambda_1^{(0)}}\mathbf{x}_{,1}^{(0)} = \mathbf{0}, \\[4mm]
-\dfrac{\Lambda^3}{\Delta^2}(F\mathbf{x}_{,1}^{(0)} - E\mathbf{x}_{,2}^{(0)}) + \dfrac{\lambda_1^{(0)}}{\lambda_2^{(0)}}\mathbf{x}_{,2}^{(0)} = \mathbf{0}.
\end{cases}
\tag{A.7}
$$

For simplicity, we assume $F = 0$ in the current configuration, which means that the moving frame $\{\mathbf{x}_{,1}^{(0)}, \mathbf{x}_{,2}^{(0)}, \mathbf{x}_N\}$ are perpendicular to each other. Then the equations (A.7) are simplified into

$$
\begin{cases}
\left(-G\dfrac{\Lambda^3}{E^2G^2} + \dfrac{\lambda_2^{(0)}}{\lambda_1^{(0)}}\right)\mathbf{x}_{,1}^{(0)} = \mathbf{0}, \\[4mm]
\left(-E\dfrac{\Lambda^3}{E^2G^2} + \dfrac{\lambda_1^{(0)}}{\lambda_2^{(0)}}\right)\mathbf{x}_{,2}^{(0)} = \mathbf{0},
\end{cases}
\tag{A.8}
$$

where the relation $\Delta = EG$ is used. Subsequently, the growth functions $\lambda_1^{(0)}$ and $\lambda_2^{(0)}$ are solved as follow

$$
\lambda_1^{(0)} = \sqrt{E}, \quad \lambda_2^{(0)} = \sqrt{G}, \tag{A.9}
$$

where the growth functions $\lambda_1^{(0)}$ and $\lambda_2^{(0)}$ just represent extension or shrinkage along the coordinate curves $\{\theta^\alpha\}$ on $\mathcal{S}_r$.

Second, we consider all components of $\mathbb{S}^{(1)}$ in (A.6) are zero

$$
\begin{cases}
\dfrac{\left(-\lambda_1^{(1)}\lambda_2^{(0)} + \lambda_1^{(0)}\lambda_2^{(1)} + \Lambda\kappa_1\right)}{\lambda_1^{(0)2}}\mathbf{x}_{,1}^{(0)} - \dfrac{\Lambda^2}{\Delta}\mathbf{x}_{,2}^{(0)} \times \mathbf{x}^{(2)} \\[2ex]
+ \dfrac{\Lambda^4}{\Delta^{5/2}}\left(N\mathbf{x}_{,1}^{(0)} - M\mathbf{x}_{,2}^{(0)}\right) + \dfrac{\lambda_2^{(0)}\left(\Delta\Lambda_{,1} - \Lambda\Delta_{,1}\right)}{\Delta^2\lambda_1^{(0)}}\mathbf{x}_N \\[2ex]
- \dfrac{\Lambda\left(\kappa_2\Lambda^2 + p^{(1)}\Delta/(2C_0)\right)}{\Delta^2}G\mathbf{x}_{,1}^{(0)} + \dfrac{\lambda_2^{(0)2}}{\Delta}\mathbf{x}_{N,1} = \mathbf{0}, \\[2ex]
\dfrac{\left(\lambda_1^{(1)}\lambda_2^{(0)} - \lambda_1^{(0)}\lambda_2^{(1)} + \Lambda\kappa_2\right)}{\lambda_2^{(0)2}}\mathbf{x}_{,2}^{(0)} + \dfrac{\Lambda^2}{\Delta}\mathbf{x}_{,1}^{(0)} \times \mathbf{x}^{(2)} \\[2ex]
- \dfrac{\Lambda^4}{Q^{5/2}}\left(M\mathbf{x}_{,1}^{(0)} - L\mathbf{x}_{,2}^{(0)}\right) + \dfrac{\lambda_1^{(0)}\left(\Delta\Lambda_{,2} - \Lambda\Delta_{,2}\right)}{\Delta^2\lambda_2^{(0)}}\mathbf{x}_N \\[2ex]
- \dfrac{\Lambda\left(\kappa_1\Lambda^2 + p^{(1)}\Delta/(2C_0)\right)}{\Delta^2}E\mathbf{x}_{,2}^{(0)} + \dfrac{\lambda_1^{(0)2}}{\Delta}\mathbf{x}_{N,2} = \mathbf{0}, \\[2ex]
\left(-\dfrac{\Lambda t_1}{\Delta} - p^{(1)}/(2C_0)\right)\mathbf{x}_N + \Lambda\mathbf{x}^{(2)} \\[2ex]
+ \dfrac{\Lambda^2}{\Delta^3}\left[\left(\Delta\Lambda_{,1} - \Lambda\Delta_{,1}\right)G\mathbf{x}_{,1}^{(0)} + \left(\Delta\Lambda_{,2} - \Lambda\Delta_{,2}\right)E\mathbf{x}_{,2}^{(0)}\right] \\[2ex]
+ \dfrac{\Lambda^3}{\Delta^2}\left(\mathbf{x}_{N,2} \times \mathbf{x}_{,1}^{(0)} - \mathbf{x}_{N,1} \times \mathbf{x}_{,2}^{(0)}\right) = \mathbf{0}.
\end{cases}
\tag{A.10}
$$

With (A.9) and $\Delta = EG$, (A.10)$_3$ is automatically satisfied and (A.10)$_1$ and (A.10)$_2$ have the following form

$$
\begin{cases}
-\left(EN + G\left(2L - E\left(2\kappa_1 + \kappa_2\right) + 2\sqrt{E}\lambda_1^{(1)}\right) + E\sqrt{G}\lambda_2^{(1)}\right)\mathbf{x}_{,1}^{(0)} = ME\mathbf{x}_{,2}^{(0)}, \\[2ex]
-\left(2EN + G\left(L - E\left(\kappa_1 + 2\kappa_2\right) + \sqrt{E}\lambda_1^{(1)}\right) + 2E\sqrt{G}\lambda_2^{(1)}\right)\mathbf{x}_{,2}^{(0)} = ME\mathbf{x}_{,1}^{(0)}.
\end{cases}
\tag{A.11}
$$

To ensure the holds of Eqs. (A.11), we need to set $M = 0$, which together with $F = 0$ ensure that the coordinate curves $\{\theta^\alpha\}$ formulate the orthogonal net of curvature lines on the target surface $\mathcal{S}_t$. Subsequently, the growth

functions $\lambda_1^{(1)}$ and $\lambda_2^{(1)}$ are obtained as follow

$$\lambda_1^{(1)} = \left(\kappa_1 - \frac{L}{E}\right)\sqrt{E}, \quad \lambda_2^{(1)} = \left(\kappa_2 - \frac{N}{G}\right)\sqrt{G}. \qquad (A.12)$$

It can be seen that the growth functions (A.9) and (A.12) are coincident with the results obtained in section 3.1.

Appendix B. Discussion on the evolution paths of the growth functions in numerical simulations

In the numerical simulations introduced in section 4, the growth functions in the growth tensors are incorporated as the state variables in the UMAT subroutine, which change gradually from 1 to the target values during the growing processes. Accompanying the change of growth functions, the growth-induced deformations of the shell samples are simulated. Intuitively, one may adopt the linear interpolations of the growth functions from 1 to the target value during the whole time regime $t \in [0, 1]$. However, this default evolution path of the growth functions may cause excessive residual stresses in the shell samples and lead to the instability phenomena. To solve this problem, we can modify the loading path of growth field $\mathbb{G}_t$ such that the residual stress can be suppressed in the growth process. To tackle the problem of instability, one possible approach is to divide the whole growing process into several stages. During each stage, the target shape of the shell or the change of the growth tensor can be prescribed properly, such that the desired deformation of the shell sample are realized. By selecting different evolution paths of the growth functions, the final shapes of the shell sample may be different.

As an illustrative example, we reconsider the generation of the apple surface through differential growth. The parametric equation (70) of the apple surface is modified into

$$
\begin{cases}
x^{(0)} = 8\cos\theta^1 \sin^2\left[\dfrac{b\pi(\theta^2 - 2)}{4}\right], \\
y^{(0)} = 8\sin\theta^1 \sin^2\left[\dfrac{b\pi(\theta^2 - 2)}{4}\right], \\
z^{(0)} = 6\sin\left[\dfrac{b\pi(\theta^2 - 2)}{2}\right],
\end{cases}
\tag{B.1}
$$

where b is a parameter to control the shape of the target surface. When $b = 1$, the parametric equation (70) of the apple surface can be recovered from Eq. (B.1). For the purpose of demonstration, we consider three evolution paths of growth functions (cf. Fig. B.1). In path 1, the growth functions λ_1 and λ_2 change linearly from 1 to those values given in Eq. (70). In paths 2 and 3, we select some intermediate points during the time regime $0 \leq t \leq 1$, such that the whole growing process into several stages (two stages in path 2 and six stages in path 3). The values of the parameter b at these intermediate points as specified as that shown in Fig. B.1. With the given value of b, the target shape of the shell in each stage can be determined from Eq. (B.1), then the change of growth tensor (or growth functions) in each stage can also be determined. Corresponding to these three evolutions paths, the simulated final shapes of the shell sample are also shown in Fig.B.1. It can be seen that the growth-induced deformation of the shell sample depends on the evolution paths. If the whole growing process is divided into more stages, the desired shape of the shell sample can be generated.
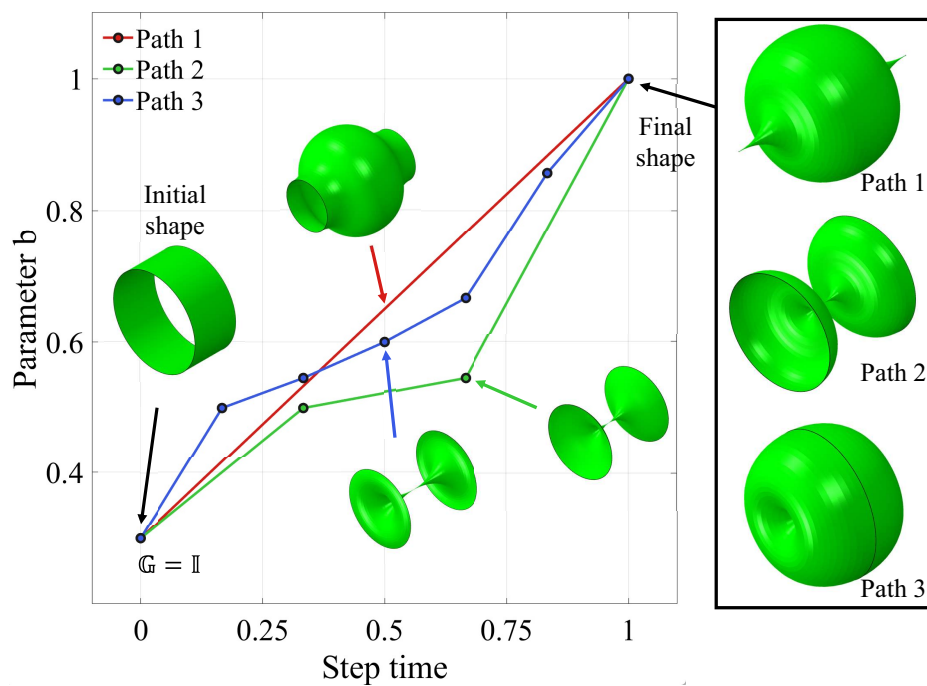
Figure B.1: The three evolution paths generated by setting the values of parameter b at some time points, and the corresponding configurations of the shell sample at the end of the growing processes.

References

Acharya, A., 2019. A design principle for actuation of nematic glass sheets. Journal of Elasticity 136, 237–249.

Ambrosi, D., Ateshian, G.A., Arruda, E.M., Cowin, S.C., Dumais, J., Goriely, A., Holzapfel, G.A., Humphrey, J.D., Kemkemer, R., Kuhl, E., 2011. Perspectives on biological growth and remodeling. Journal of the Mechanics and Physics of Solids 59, 863–883.

Ben Amar, M., Goriely, A., 2005. Growth and instability in elastic tissues. Journal of the Mechanics and Physics of Solids 53, 2284–2319.

Chen, W.H., 2017. Differential geometry (2nd Edition). Peking University Press.

Ciarlet, P.G., 2005. An introduction to differential geometry with applications to elasticity. Journal of Elasticity 78, 1–215.

Dai, H.H., Song, Z., 2014. On a consistent finite-strain plate theory based on three-dimensional energy principle. Proceedings of the Royal Society A: Mathematical, Physical and Engineering Sciences 470, 20140494.

Dias, M., Hanna, J., Santangelo, C., 2011. Programmed buckling by controlled lateral swelling in a thin elastic sheet. Physical Review E 84, 036603.

Dortdivanlioglu, B., Javili, A., Linder, C., 2017. Computational aspects of morphological instabilities using isogeometric analysis. Computer Methods in Applied Mechanics and Engineering 316, 261–279.

Gladman, A.S., Matsumoto, E.A., Nuzzo, R.G., Mahadevan, L., Lewis, J.A., 2016. Biomimetic 4d printing. Nature materials 15, 413–418.

Goriely, A., 2017. The Mathematics and Mechanics of Biological Growth. Springer, New York, NY.

Goriely, A., Ben Amar, M., 2005. Differential growth and instability in elastic shells. Physical Review Letters 94, 198103.

Groh, R.M., 2022. A morphoelastic stability framework for post-critical pattern formation in growing thin biomaterials. Computer Methods in Applied Mechanics and Engineering 394, 114839.

Huang, C., Wang, Z., Quinn, D., Suresh, S., Hsia, K.J., 2018. Differential growth and shape formation in plant organs. Proceedings of the National Academy of Sciences of the United States of America 115, 12359–12364.

Hwang, D., Barron, E.J., Haque, A.B.M.T., Bartlett, M.D., 2022. Shape morphing mechanical metamaterials through reversible plasticity. Science robotics 7, eabg2171.

Jones, G.W., Mahadevan, L., 2015. Optimal control of plates using incompatible strains. Nonlinearity 28, 3153–3174.

Kadapa, C., Li, Z., Hossain, M., Wang, J., 2021. On the advantages of mixed formulation and higher-order elements for computational morphoelasticity. Journal of the Mechanics and Physics of Solids 148, 104289.

Kempaiah, R., Nie, Z., 2014. From nature to synthetic systems: shape

transformation in soft materials. Journal of Materials Chemistry B 2, 2357–2368.

Kondaurov, V., Nikitin, L., 1987. Finite strains of viscoelastic muscle tissue. Journal of Applied Mathematics and Mechanics 51, 346–353.

Li, B., Cao, Y.P., Feng, X.Q., Gao, H., 2011. Surface wrinkling of mucosa induced by volumetric growth: Theory, simulation and experiment. Journal of the Mechanics and Physics of Solids 59, 758–774.

Li, B., Cao, Y.P., Feng, X.Q., Gao, H., 2012. Mechanics of morphological instabilities and surface wrinkling in soft materials: a review. Soft matter 8, 5728.

Li, Y., Dai, H.H., Wang, J., 2019. On a consistent finite-strain shell theory for incompressible hyperelastic materials. Mathematics and Mechanics of Solids 24, 1320–1339.

Li, Z., Wang, Q., Du, P., Kadapa, C., Hossain, M., Wang, J., 2022. Analytical study on growth-induced axisymmetric deformations and shape-control of circular hyperelastic plates. International Journal of Engineering Science 170, 103594.

Liu, Y., Genzer, J., Dickey, M.D., 2016. "2d or not 2d": shape-programming polymer sheets. Progress in Polymer Science 52, 79–106.

Liu, Z.S., Toh, W., Ng, T.Y., 2015. Advances in mechanics of soft materials: a review of large deformation behavior of hydrogels. International Journal of Applied Mechanics 07, 1530001.

Mehta, S., Raju, G., Saxena, P., 2021. Growth induced instabilities in a circular hyperelastic plate. International Journal of Solids and Structures 226-227, 111026.

Nojoomi, A., Jeon, J., Yum, K., 2021. 2d material programming for 3d shaping. Nature Communications 12, 603.

Pezzulla, M., Stoop, N., Steranka, M.P., Bade, A.J., Holmes, D.P., 2018. Curvature-induced instabilities of shells. Physical review letters 120, 048002.

Rausch, M.K., Kuhl, E., 2014. On the mechanics of growing thin biological membranes. Journal of the Mechanics and Physics of Solids 63, 128–140.

Rodriguez, E.K., Hoger, A., McCulloch, A.D., 1994. Stress-dependent finite growth in soft elastic tissues. Journal of Biomechanics 27, 455–467.

Siéfert, E., Reyssat, E., Bico, J., Roman, B., 2019. Bio-inspired pneumatic shape-morphing elastomers. Nature materials 18, 24–28.

Song, Z., Dai, H.H., 2016. On a consistent finite-strain shell theory based on 3-d nonlinear elasticity. International Journal of Solids and Structures 97-98, 137–149.

Souhayl Sadik, Arzhang Angoshtari, Alain Goriely, Arash Yavari, 2016. A geometric theory of nonlinear morphoelastic shells. Journal of Nonlinear Science 26, 929–978.

Steigmann, D.J., 2012. Extension of koiter's linear shell theory to materials

exhibiting arbitrary symmetry. International Journal of Engineering Science 51, 216–232.

Tao, Y., Lee, Y.C., Liu, H., Zhang, X., Cui, J., Mondoa, C., Babaei, M., Santillan, J., Wang, G., Luo, D., Di Liu, Yang, H., Do, Y., Sun, L., Wang, W., Zhang, T., Yao, L., 2021. Morphing pasta and beyond. Science advances 7.

Toponogov, V.A., 2006. Differential geometry of curves and surfaces. Birkhäuser Boston.

van Manen, T., Janbaz, S., Zadpoor, A.A., 2018. Programming the shape-shifting of flat soft matter. Materials Today 21, 144–163.

van Rees, W.M., Vouga, E., Mahadevan, L., 2017. Growth patterns for shape-shifting elastic bilayers. Proceedings of the National Academy of Sciences 114, 11597–11602.

Vetter, R., Stoop, N., Jenni, T., Wittel, F.K., Herrmann, H.J., 2013. Subdivision shell elements with anisotropic growth. International Journal for Numerical Methods in Engineering 95, 791–810.

Wang, J., Li, Z., Jin, Z., 2022. A theoretical scheme for shape-programming of thin hyperelastic plates through differential growth. Mathematics and Mechanics of Solids , 108128652210896.

Wang, J., Song, Z., Dai, H.H., 2016. On a consistent finite-strain plate theory for incompressible hyperelastic materials. International Journal of Solids and Structures 78-79, 101–109.

Wang, J., Steigmann, D., Wang, F.F., Dai, H.H., 2018. On a consistent finite-strain plate theory of growth. Journal of the Mechanics and Physics of Solids 111, 184–214.

Wang, J., Wang, Q., Dai, H.H., Du, P., Chen, D., 2019a. Shape-programming of hyperelastic plates through differential growth: an analytical approach. Soft Matter 15, 2391–2399.

Wang, J., Wang, Q., Dai, H.H., Du, P., Chen, D., 2019b. Shape-programming of hyperelastic plates through differential growth: an analytical approach. Soft matter 15, 2391–2399.

Wex, C., Arndt, S., Stoll, A., Bruns, C., Kupriyanova, Y., 2015. Isotropic incompressible hyperelastic models for modelling the mechanical behaviour of biological tissues: a review. Biomedizinische Technik. Biomedical engineering 60, 577–592.

Xu, F., Fu, C., Yang, Y., 2020. Water affects morphogenesis of growing aquatic plant leaves. Physical review letters 124, 038003.

Yu, X., Fu, Y., Dai, H.H., 2020. A refined dynamic finite-strain shell theory for incompressible hyperelastic materials: equations and two-dimensional shell virtual work principle. Proceedings. Mathematical, physical, and engineering sciences 476, 20200031.

Yu, X., Zhong, X., Chen, X., 2022. On an asymptotic shell model for growth-induced finite deformations. unpublished results .